Integration of a Bimorph Thermal Microactuator with Electrostatically Actuated Nano Tweezers

by

Mehmet Yılmaz

A Thesis Submitted to the
Graduate School of Engineering
in Partial Fulfillment of the Requirements for
the Degree of

Master of Science
in
Mechanical Engineering

Koc University

August 2007

Koc University

Graduate School of Sciences and Engineering

This is to certify that I have examined this copy of a master's thesis by

Mehmet Yılmaz

and have found that it is complete and satisfactory in all respects,
and that any and all revisions required by the final
examining committee have been made.

Committee Members:

_____

B. Erdem Alaca, Ph. D. (Advisor)

_____

Arda D. Yalçınkaya, Ph. D.

_____

Gürer G. Budak, M.D., Ph. D.

Date: _____

ABSTRACT

The engineering of the integration of micro-scale structures with nano-scale objects such as nanowires, nanoparticles, and carbon nanotubes is one of the most vibrant and challenging research fields due to the strong promise it entails for today's and future applications including nano manipulation, biotechnology, and cell/molecule manipulation.

This study is geared towards MEMS gripper design and prototype fabrication for the demonstration of the following issues:

1) The intentional integration of micro-scale comb-actuator grippers with nanowires as end-effectors, and
2) The integration of electrostatic and thermal actuators for better gripping capability.

Three process flows are developed, one of which is chosen for demonstration. The micro/nano integration even during a sophisticated device fabrication such as a gripper with both electrostatically and thermally actuated end-effectors is realized at the end.

The micro/nano integration method used in this study is inspired by the techniques called PADOX (Pattern Dependent Oxidation) and sequential DRIE (Deep Reactive Ion Etching). Both techniques are size reduction methods based on the oxidation of silicon structures followed by oxide etch. Through PADOX one obtains a single nanowire out of a bigger silicon structure, whereas in sequential DRIE a vertical stack of such nanowires is obtained by utilizing the scalloping effect.

On the other hand, the integration of thermal and electrostatic actuation mechanisms is realized by using a three mask monolithic process. First mask is used to define the silicon electrostatic actuator on SOI wafer. Second mask is used to obtain the bimorph thermal microactuator made of polyimide and aluminum layers on top of the electrostatic actuator. Third and the final mask is used to release the integrated electrostatic and thermal microactuators.

Keywords: MEMS, integration, micro/nano integration, batch compatibility, nanotweezers, nanowire, comb actuator, comb-finger, bimorph thermal actuator, scalloping effect.

ÖZET

Mikro ölçekli yapıların, kontrollü olarak, nanotel, nano parçacık, ve karbon nanotüpler gibi nano ölçekli yapılar ile integrasyonunun mumkun olmasi ve nanomanipulasyon, biyoteknoloji ve hücre/molekül manipulasyonu gibi alanlardaki yüksek olasilikli uygulanabilir oluşu bu konunun günümüzde ve gelecekte en hareketli, canli ve zorlu araştirma alanlarından bir tanesi olmasını sağlamaktadır.

Bu çalışma bir MEMS tutucusunun tasarımını ve prototip üretimi esnasında karşılaşılmış olan aşağıdaki problemlerin çözümlenmesini ana çerçeve olarak kabul etmiştir:

1) Mikro-ölçekteki elektrostatik tahrik ile çalışan tutuculara nano-ölçekli yapıların integrasyonu, ve
2) Farklı tahrik mekanizmalarına sahip iki mikro aletin birbirine integrasyonu.

Problemin çözümü için üç tane üretim şeması geliştirilmiş, ve bunlardan bir tanesi örnek olay incelemesi olarak ele alınmıştır. Üretim işleminin sonunda, mikro/nano integrasyonun çok karmaşık bir üretim süreci içinde de yapılabildiği ispatlanmıştır.

Bu çalışmada kullanılmış olan mikro/nano integrasyon yöntemi PADOX (Pattern Dependent Oxidation) ve sıralı olarak yapılan DRIE (Deep Reactive Ion Etching) işlemlerinden esinlenilerek oluşturulmuştur. Her iki yöntem de, silisyum yapıların oksitlendirilerek, oluşan oksidin silisyum yapı etrafından dağlanarak uzaklaştırılması mantığını temel olarak almaktadır. PADOX yöntemi ile sadece bir tane nanotel elde ediliyorken, sıralı olarak yapılan DRIE yöntemi ile düşey doğrultuda sıralanmış nanotel dizisi “scalloping effect” denilen olay sonucunda elde edilebiliyor.

Diğer taraftan ise, ısıl tahrik ve elektrostatik tahrik ile çalışan iki mekanizmanın integrasyonunda üç maskelik bir monolitik proses takip edilmiştir. Birinci maske ile SOI alttaş üzerindeki silisyum elektrostatik tahrik mekanizması oluşturulmuş, ikinci maske ile de polyimide ve alüminyum tabakalarından oluşan ısıl tahrik mekanizması elde edilmiştir.

Üçüncü ve son maske ile de, her iki tahrik mekanizmasını da içerisinde barındıran mikro alet isotropik dağlama ile etrafındaki oksit ve silisyum tabakalarından temizlenerek tahrik edilebilir hale getirilmiştir.

Anahtar Kelimeler: MEMS, integrasyon, mikro/nano integrasyon, seri üretim, nanocımbız, nanotel, elektrostatik tahrik, ısıl tahrik.

ACKNOWLEDGEMENTS

This wonderful thesis study became a part of my life for the last 2 years… I believe that, I will feel the effects of this thesis study in my coming life with its all contributions.

I would like to deeply thank my advisor Dr. Erdem Alaca for his belief and trust about my decisions, my personality, and for his outstanding help during the most difficult parts of the design and microfabrication of the devices; Also, to Dr. Arda Yalçınkaya for his valuable advices during the discussions about design and fabrication of my thesis studies. Although he is not my official advisor or co-advisor, I would like to call him as my co-advisor since I felt that he gave me advice as he was my co-advisor.

Next, I would like to deeply thank to Prof. Yusuf Leblebici for his contributions to my thesis studies, because he opened a gate to a wonderful experience in the facilities of CMI at EPFL; to Dr. Gürer Budak for being a committee member in my thesis defense, and for his valuable criticism about my work and contribution about the potential application areas of the devices in the field of nanobiotechnology and nanomedicine.

I would like to deeply thank to Mihalis Zervas for his outstanding effort during the last process flow design, the microfabrication of the devices in the facilities of CMI, and valuable discussions about the encountered problems and their solutions; to Özlem Şardan for her patience while listening to my questions, and answering them by waiving from her very valuable time; to my laboratory friend Özgür Özsun for his scientific support, and to Çağlar Ataman for his support during constructing the characterization setups, to TUBITAK because of their pecuniary support in my thesis studies.

This study is supported in part by TUBITAK under grant No.104 M216.

I kept the most valuable part to the end… I dedicate this study to my all family because of their patience. To my grandmother for her endless praying, to my mother and father for their endless support and always being with me, and to my elder brother for navigating me to the way, and paying effort to always keep me there… You are all priceless for me…

TABLE OF CONTENTS

LIST OF TABLES

LIST OF FIGURES

NOMENCLATURE

C : Capacitance, or Rayleigh Number dependent Coefficient

ε : Permittivity of the material in the gap between two parallel plates

ε_0 : Free space permittivity

A : Engagement area between two parallel plates, and

g : Gap between the plates of the parallel plate capacitor.

W : Stored Energy

C_T : Total Capacitance

V : Applied Voltage Difference

h : Height of comb-finger

d : Distance between two comb-fingers, or Out-of-plane tip deflection of a bimorph thermal actuator

N : Number of comb-fingers

x : Moved distance

x_e : Engagement distance

w_f : Finger width

F_{ES} : Electrostatic force

F_{MECH} : Mechanical force

k_{MECH} : Mechanical spring constant

E : Young's Modulus

h_s : Spring Height

w_s : Spring Width

l_s : Spring Length.

ΔT : Temperature difference

L : Length of a thermal actuator, or plate which has convective heat ransfer

$m : h_1 / h_2$, where h_1, h_2 represent the *lower and upper layer thickness respectively*,

$n : E_1 / E_2$, where E_1, E_2 represent elastic modules of materials used in a thermal actuator

α_1, α_2 : Coefficient of thermal expansions (CTEs) of materials used in a thermal actuator

α : Thermal diffusivity [m^2/s]

Ra_L : Rayleigh Number

g : Gravity

$\beta = T_f^{-1}$: Film temperature

T_s : Surface Temperature

T_∞ : Environment (Fluid) Temperature

ν : Kinematic viscosity [m^2/s]

$\overline{Nu_L}$: Nusselt Number

$\bar{h}$: Average convection coeff.

k : Thermal conductivity

n : Rayleigh Number dependent exponent

Chapter 1

INTRODUCTION

1.1 Introduction

Micro/nano technologies are one of the most challenging and wide research fields. *Integration of microstructures with nanostructures* is one of these research fields. There is wide research and very different approaches that aim to find solutions for *micro/nano integration.* This thesis study proposes a novel solution for the integration of micro and nano scaled structures while the only aim during the process was not the integration of micro/nanostructures.

1.2 Aim

Although there are a lot of different methods to fabricate nanostructures integrated to substrate surfaces, engineered integration of nanostructures to microdevices is very challenging due to the problems encountered during microfabrication processes. These problems are a part of the process and are in the nature of the microfabrication. In other words, there is no easy way for the integration, and the game should be played with the rules of the nature.

We have tried to solve this micro/nano integration difficulty by proposing three different methods and finally demonstrated the simplest, and most time efficient approach due to the limited time.

The most serious difficulty about micro/nano integration comes from lack of protection of the nanostructures during the sequential aggressive steps of microfabrication relative to

the fabrication of microdevices or microstructures. In this thesis study, we experienced this problem in all the methods that we proposed, however we always found a way to protect the nano side of the devices from the aggressive environment of microfabrication processes.

According to the information given above, the most serious aim of this thesis study was finding a way for the demonstration of “nano end-effectors” / “microgripper” integration.

Another aim of this thesis study was to demonstrate the integration of two different microdevices with different actuation mechanisms to obtain both in-plane and out-of-plane motion types in order to obtain a better gripping action compared to the similar devices with only in-plane motion ability. Although this aim seems as a very simple idea it was not encountered in the literature survey, and become an attractive aim to demonstrate the possibility of the idea and opened a way for different applications in minds of other researchers in the field. We have found several approaches that use bimorph thermal actuation, or electrostatic actuation mechanisms for in-plane motion or out-of-plane motion. However, both of them are not used integrated to each other together.

What making this study more promising is the potential behind this application to use next generation of the devices fabricated in this study as tweezers for appropriate biotechnological applications, after addressing problems related with working in liquid environment of biotechnology.

Although it is out of the scope of this thesis study, the ultimate goal related to this micro/nano integration in tweezers applications of our group is to manipulate biological cells and organic molecules, and/or investigate the force interactions between biological cells and finally between organic molecules.

There is a wide research about bionanotechnology and biotechnology. Because of this, there is a lot of demand for micro/nanodevices that can perform tasks in cellular and molecular scale. According to one of the principal investigators in the field, Prof. Gang

Bao, the devices that we worked on are promising applications for the investigation of cell behavior to external mechanical forces [1]. However, at first, very fundamental problems related to investigation of cells in their natural environment, which is working in medical liquid environment, should be addressed.

1.3 Inspiration for Nanowire Fabrication

The integration method which we use in this study is an inspiration from [2], [3], and [4]. Doherty et. al., [4] used sequential Deep Reactive Ion Etching (DRIE) steps, and followed these steps with thinning of silicon structures with oxidation. After the oxidation of silicon, dimensions of the silicon structures are reduced, and following this oxidation, the process is finished by etching of the oxide at the outer surface of the silicon nanostructures. Pott et. al., [2], used the technique called as PADOX (Pattern Dependent Oxidation (Pioneered by Takahashi [3])) to obtain silicon nanowires. At the beginning of the process, they used an oxide hard mask to define the initial shape of silicon structure, which will be used as the shape to produce the final silicon nanowires. After obtaining these structures, they oxidized these silicon structures to obtain the final, smaller radii nanowires. There is an important thing to emphasize about obtaining these silicon nanowires by oxidation. Although, there were no wire shaped structures prior to the beginning of the oxidation (The shapes were nanowall like structures), there is a final wire shaped silicon nanowire due to the phenomena known as “decrease in the oxidation rate inside the stressed silicon”. This idea is the fundamental reason behind obtaining nanowires with this method, and is used to obtain these nanowires by Pott et.al.

1.4 A Brief Literature Review for Thermal Actuators

Thermal actuators are used in different applications with different purposes.

For example, [5], and [6] used thermally actuated polymer microrobotic grippers for manipulation of biological cells. A trimorph thermal actuator, with one heating layer and two layers with different CTEs (Coefficient of Thermal Expansions), was used to demonstrate that the manipulation is possible. The heater layer is covered with the other two layers in order to allow for the actuation of the device in ionic liquids. [7] aimed to use a bimorph thermal actuation mechanism for a similar application. The main difference was the behavior of the device to the applied current flow in the electrically conductive layer. In this application, [7], the bimorph device is initially prebent because of the internal stresses, and when a current flow is generated the thermal actuators are flattened. Different than the other devices, this device can also be actuated with electrostatic attraction. When a voltage difference between the substrate surface and the device is applied, the prebent device approaches to the substrate surface due to the electrostatic attraction. [8] used bimorph thermal actuation both for in-plane and out-of-plane motion of a 3D scanner application. The materials that they used are bulk silicon and evaporated aluminum that was deposited on the sidewalls of the beam shaped silicon structures. [9] used serially and parallel connected thermal actuators to obtain ciliary motion to transfer objects from one place to another place.

The main disadvantage of bimorph thermal actuators is the risk of delamination due to weak interface connection between the layers of the bimorph during repeated actuation of the device. [10] proposed an interesting solution to this issue, with a drawback of loss in force generated by the device actuation. In bimorph thermal actuators, the interface is not at the zero strain plane, but at a different plane. They, use a buffer layer to move the zero stain layer to one of the interfaces of the trilayer thermal actuator. It is important to emphasize that, at the beginning the actuator was a bilayer, and the thermal actuator is modified to a

trilayer thermal actuator after the addition of the buffer layer. This buffer layer is used to obtain strong bonds between the interfaces and to shift the neutral plane to the weak interface of the trilayer actuator.

1.5 Outline

This thesis report is composed of 6 chapters.

The first chapter is dedicated for an introduction about the aim of the study and possible future applications of nanotweezers. A brief literature review is done to give a wide idea about the possible applications using thermal bimorph/trimorph actuators.

Second chapter is used in order to explain the theory of the two actuation mechanisms that we use in this thesis study. Furthermore, electrostatic actuator and thermal actuator device parameters are given here, and the reasons to choose these parameters are described.

In third chapter, three fabrication sequences for integration of devices with different actuation mechanisms are explained. In these fabrication sequences, micro/nano integration is, also, proposed. Finally, the reasons to choose the last fabrication sequence as a case study are given.

Fourth chapter is dedicated to explain the method we followed when we were designing the layout for the microfabrication of the Cr masks, which were used to fabricate the real devices.

In chapter 5, at first the reasons to follow generation based microfabrication process are explained (We made 1st and 2nd Generation devices). Also, the procedure followed during the microfabrication of the devices is explained with micrographs from real devices. Furthermore, the problems we encountered during the microfabrication of the 1st Generation devices were addressed.

The sixth and the last chapter of the thesis study in used to explain the conclusions obtained from this study. A discussion section is used to evaluate the results, and an advice section is included to help future scientists planning to work on the same or similar fields.

Chapter 2

PRINCIPLES OF ACTUATION MECHANISMS AND DEVICE DESIGN

2.1 Introduction

Here, we present the working principles of the nanotweezers that utilize both electrostatic and thermal actuation mechanisms to achieve a better gripping action, and give the design parameters that we use in the masks. Similar to the previous device, which was studied at Koc University [11], electrostatic actuation is used to drive end-effectors within the plane of the device, whereas the integrated thermal actuator is now introduced as a thumb that counteracts both end-effectors. The integration of the thermal actuator is expected to improve grabbing ability of the complete nanotweezers.

2.2 Electrostatic Actuation Mechanism

The electrostatic actuation mechanism is extensively explained in [11], [12], and [13]. The basic idea behind the working principle is the actuation (movement) due to the electrostatic attraction between two surfaces (or objects) that have different electrical potentials with respect to each other. In order to explain the mechanism in a better way, see Figure 2.1, and follow the explanations written below.

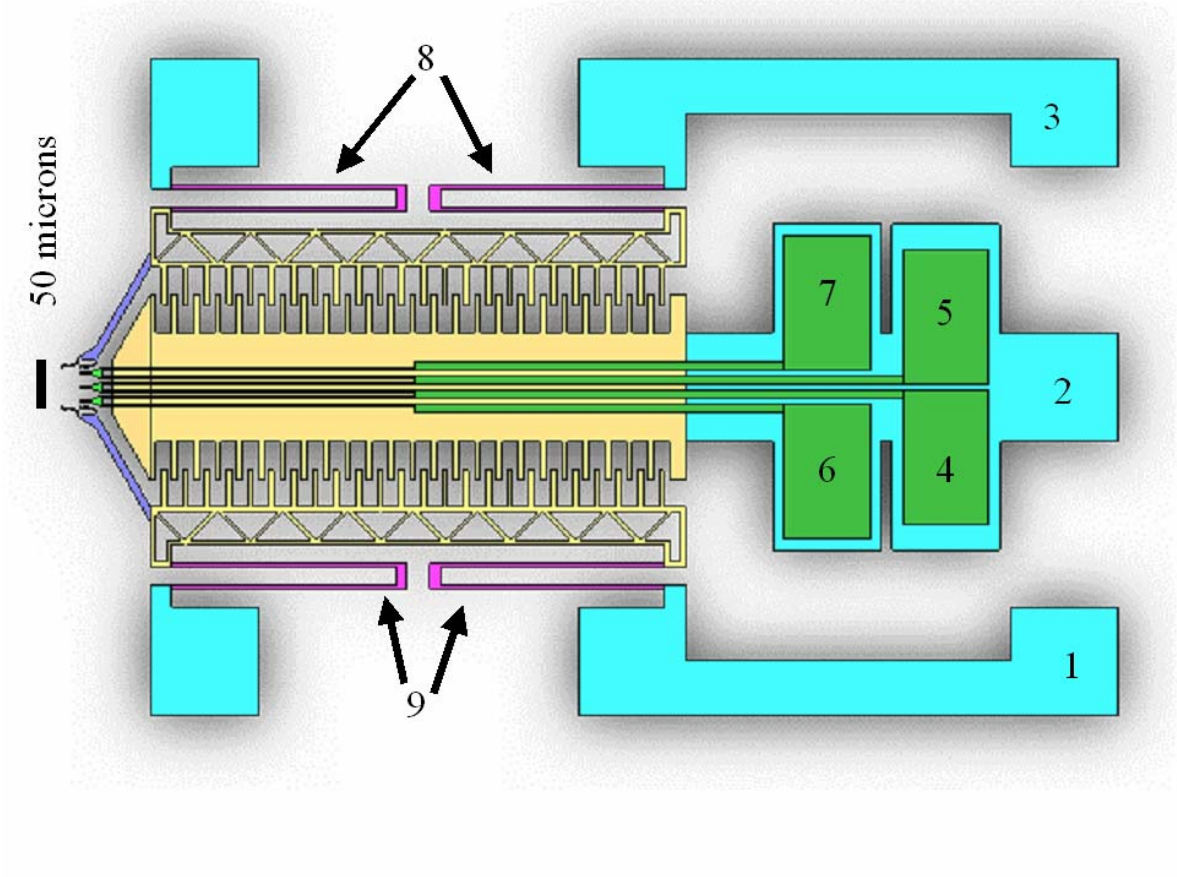

Figure 2. 1: Explanation of electrostatic actuation mechanism

For the electrostatic actuation mechanism there are 3 touch pads (Numbered as 1, 2, and 3). These touch pads are used to electrostatically load parts of the device with the required electrical potentials. For example, loading touch pad #1 with V=40 Volts, and touch pad#2 with V=0 Volts causes an attraction between base part of the device and the left movable part of the device. As a result, the left movable part approaches to the base part of the device until the movable part stops because of the force generated by the deformation of the mechanical springs (Mechanical springs are numbered as 8, and 9). Thus, the force generated due to the deformation of the mechanical springs balances the

generated electrostatic attraction force. In other words, the movement due to the electrostatic attraction between two objects continues until the deformation of the mechanical springs causes the same, but opposite mechanical force.

After this simple summary of the electrostatic actuation mechanism, we go on with a more scientific explanation, which is well explained in [12].

2.2.1 Capacitors and Comb-finger Actuators

Capacitance of a parallel plate capacitor (Figure 2.2) is defined as

$$C = \varepsilon A / g = \varepsilon th / g , \qquad (2.1)$$

where,

ε : Permittivity of the material in the gap between two parallel plates,

A : Engagement area between two parallel plates, and

g : Gap between the plates of the parallel plate capacitor.

In our case, and most MEMS applications, gap volume is filled with air, permittivity of which is $\varepsilon \approx \varepsilon_0 = 8.854 * 10^{-12} F / m$.

Instantaneous energy stored in a parallel plate capacitor when a voltage difference is applied to the plates of the capacitor is

$$W = \frac{1}{2} C_T V^2 . \qquad (2.2)$$

Where,

W : Stored Energy, C_T : Total Capacitance, V : Applied Voltage Difference.

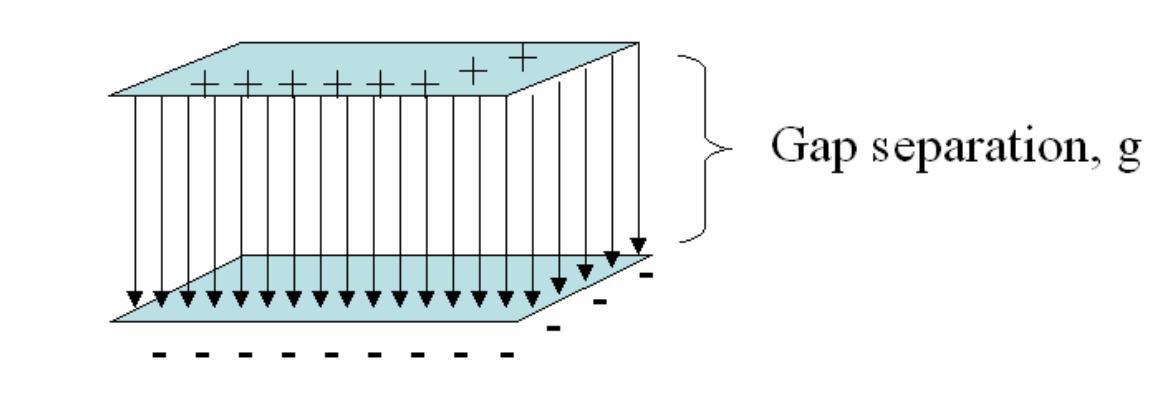

Figure 2. 2: A parallel plate capacitor

It is also possible to use this formula for comb-finger actuators (Figure 2.3). By using the same method, it is possible to make an approximation by dividing a comb-finger *pair* actuator to four parallel plate capacitors. We can divide these four capacitors into two groups. These two groups are:

1. Capacitance in the desired actuation direction, which is assumed as parasitic capacitance, and
2. Capacitance in the lateral instability direction, which is the desired capacitance.

For the comb-finger *pair* actuator,

$$C_T = C_I + C_P , \tag{2.3}$$

where,

$$C_I(x) = 2N\varepsilon_0 \frac{h}{d}(x_e + x) , \tag{2.4}$$

and

$$C_P(x) = 2N\varepsilon_0 h \frac{w_f}{x_f - x} . \tag{2.5}$$

Taking the minus derivative of the instantaneous energy stored in the system we find the electrostatic force attracting the movable comb-finger towards the fixed comb-fingers as:

$$F_{ES} = -\left.\frac{\partial W}{\partial x}\right|_{V} = -(N\varepsilon_0 \frac{h}{d} V^2 + N\varepsilon_0 h \frac{w_f}{(x_f - x)^2} V^2) \qquad (2.6)$$

When there is equilibrium, this generated electrostatic force is equalized by the restoring mechanical force, F_{MECH}. The reason for the restoring mechanical force, F_{MECH}, is the mechanical deformation of the beam type springs. The magnitude of the generated mechanical force, F_{MECH}, is *displacement due to the mechanical deformation of the spring* times *mechanical spring constant of the spring.* In mathematical form:

$$F_{MECH} = k_{MECH} x \qquad (2.7)$$

where,

x: Displacement due to the mechanical deformation of the spring, and

k_{MECH}: Mechanical spring constant of a beam type spring.

Mechanical spring constant of a beam is defined as:

$$k_{MECH} = \frac{E h_s w_s^3}{l_s^3}, \qquad (2.8)$$

where,

E: Young's Modulus, h_s: Spring Height, w_s: Spring Width, and l_s: Spring Length.

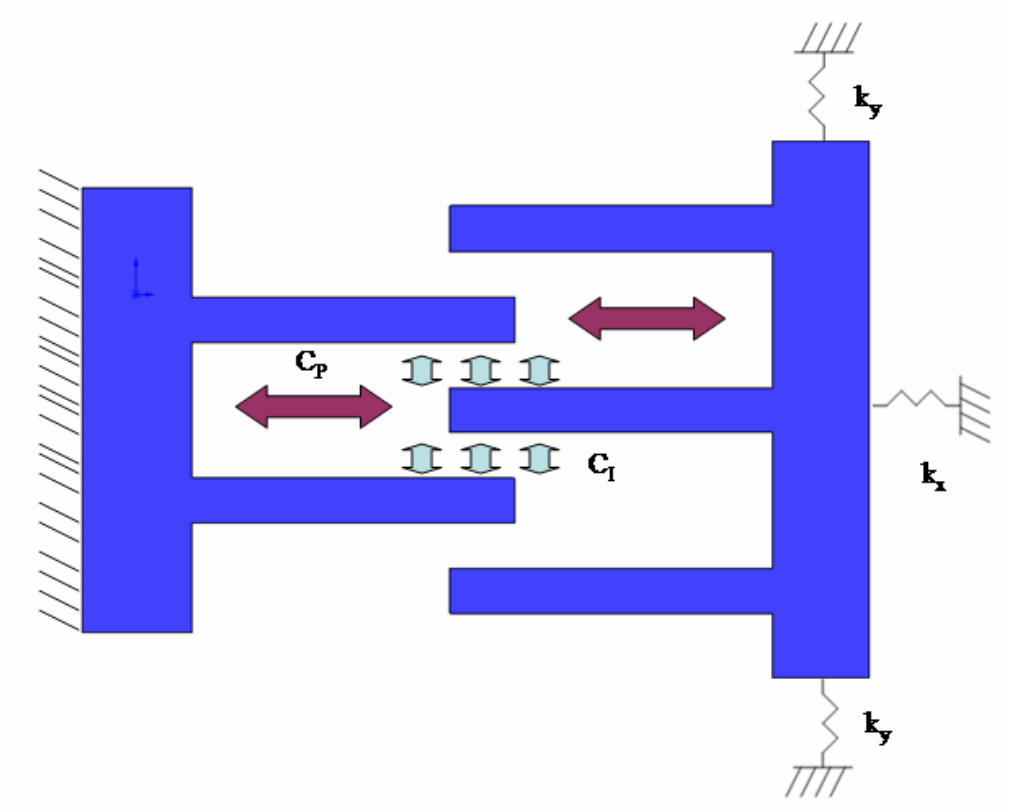

Figure 2. 3: A comb-actuator pair

2.2.2 Instability types

There is a phenomena called as *pull-in* for parallel plate capacitors and comb-finger actuators. It is very important to emphasize that the pull-in phenomena in capacitors and comb-actuators are not exactly the same mechanisms. There are two differences between the *pull-in* phenomena in parallel plate capacitors and comb-finger actuators:

1. Parallel plate capacitors have a characteristic pull-in displacement of 1/3 of the initial gap distance, while the pull-in displacement of comb-actuator mechanisms need to be calculated every time as somebody designs comb-actuators with different comb-finger geometries,

2. Comb-finger actuators mostly suffer because of the lateral instability rather than the displacement in the desired direction [14]. In other words, the first type of instability that comb-actuators encounter is *pull-in problems due to lateral instabilities* rather than instabilities related to the desired direction of motion.

Related with the second entry in the explanation above, it is possible to say that: As comb-finger pairs approach to each other, the parallel plate capacitor behavior of the comb-finger pairs become significant, and in order to reduce the possibility of lateral instability, comb-finger actuators should be designed with different geometries as suggested in [15], [16], [17], [18], [19], [20], [21], and [22], and the comb-fingers should be made stiffer than the regular comb-fingers to hinder the bending of the comb-fingers due to large lateral forces.

2.3 Bimorph Thermal Actuation Mechanism

Working principle of a thermal actuator is to bond two materials with different Coefficient of Thermal Expansions (CTEs), and to increase the temperature of these materials. Assuming that these materials are initially flat, and at the same temperature after they are bonded, the materials will bend after their temperature is increased or decreased in an amount of ΔT (Figure 2.5). This is the simplest working principle for a thermal actuator.

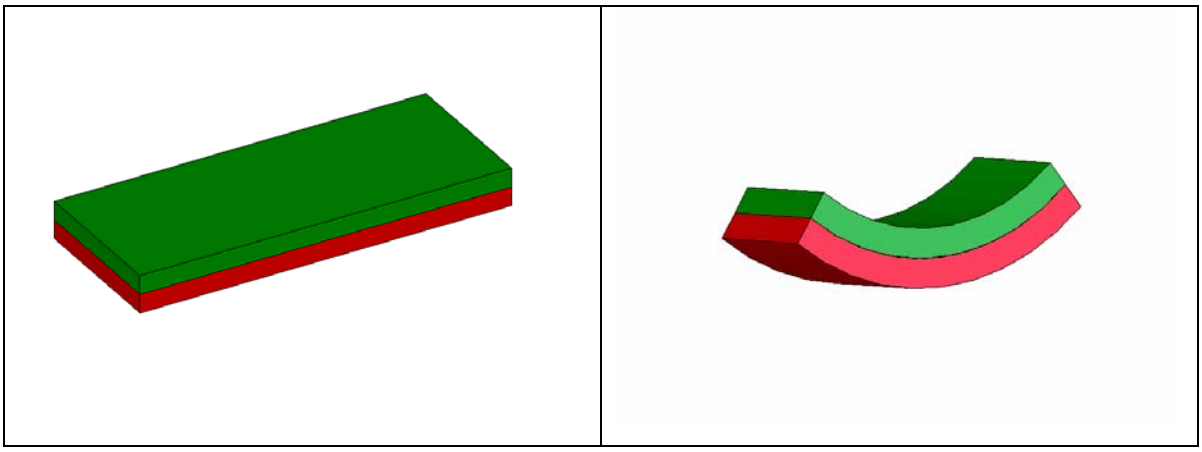

Figure 2. 4: Bonded materials, flat, and initially at same temperature (left), temperature is increased/decreased in an amount of ΔT (right).

There are three ways to excite a bimorph thermal actuator, either by passing a current through the conductor material between two touch pads of a thermal actuator, or by completely increasing the temperature of the environment and thermal actuator at the same time [5], or focusing a light beam to a certain point on the actuator by a lens sequence, and increase the temperature of the materials with different CTEs by conduction [18]. The thermal actuator mechanism that we are working on has the ability to work with the actuation mechanisms of [5].

2.3.1 Analytical Thermo-Mechanical Treatment

References [23], and [24] give the displacement formulas for a bimorph thermal actuator as shown below.

$$d = \frac{L^2}{(h_1 + h_2)} . \frac{3(1+mn)^2}{[3(1+m)^2 + (1+mn)(m^2 + 1/(mn))]} . (\alpha_1 - \alpha_2) . \Delta T , \qquad (2.9)$$

or similarly expressed as:

$$d = \frac{L^2}{h_2} . \frac{3(1+mn)}{[3(1+m)^2 + (1+mn)(m^2 + 1/(mn))]} . (\alpha_1 - \alpha_2) . \Delta T . \qquad (2.10)$$

Where,

d : Out-of-plane tip deflection of a bimorph thermal actuator,

L : Length of a thermal actuator,

$m : h_1 / h_2$, where h_1, h_2 represent the *lower and upper layer thicknesses respectively*,

$n : E_1 / E_2$, where E_1, E_2 represent elastic modules of materials used in a thermal actuator,

α_1, α_2 : Coefficient of thermal expansions (CTEs) of materials used in a thermal actuator,

ΔT : Temperature difference between initial and final states of bonded thermal actuator materials.

We have chosen aluminum and a polyimide (PI), PI2610 (Trade Mark of HD Microsystems), as layers of the thermal actuators in our design. The most important material property that we have considered during the selection of the materials for the thermal actuators was the CTEs of materials in order to obtain the maximum possible tip deflection [25]. CTEs of Al and PI2610 are 23.1 ppm/K and 3 ppm/K, respectively. In addition, there are other reasons, such as high dielectric strength, to choose PI as the thermal actuator material.

According to various physical confinements, we must have approximately 1 to 2 μm tip deflection with a thermal actuator length of $L : 35 \sim 60 \mu m$. The reason for 1 to 2 μm tip deflection is the intentional level difference between tip of the thermal actuator when it is at rest position and when it is thermally actuated for the purpose of grabbing an object. Lower layer of the thermal actuator is over an oxide layer (The oxide layer is composed of 200nm thermally grown oxide, 1 micron LTO and 1.5 micron deposited BPSG with reflow at 1050 C°). And, 1-micron thick Aluminum layer is on 2-micron thick PI2611 layer of the thermal actuators (See Figure 2.6).

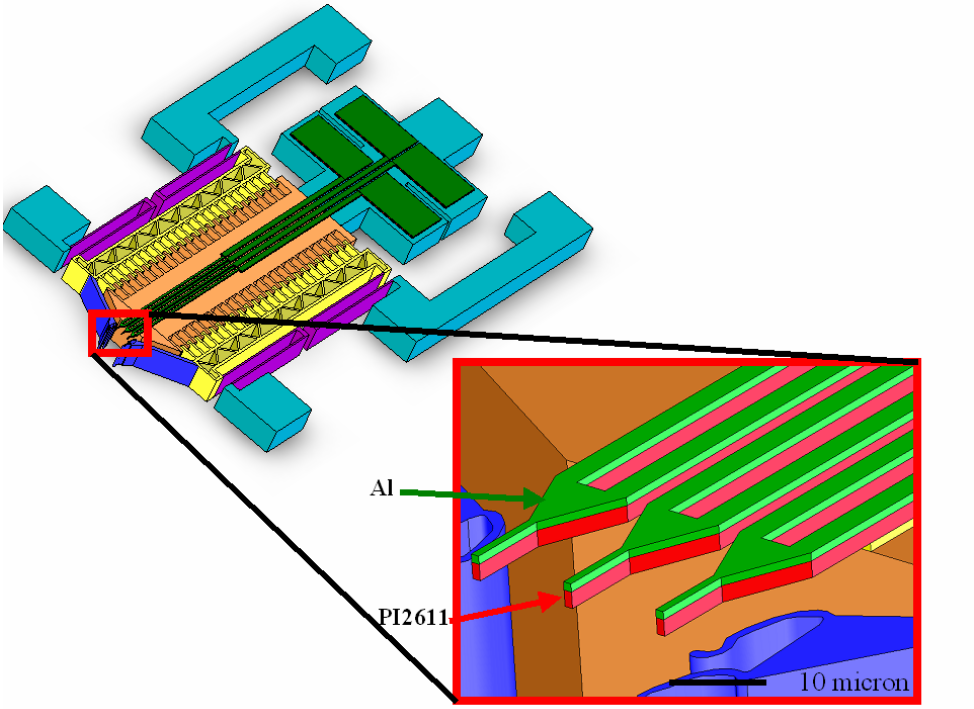

Figure 2. 5: Layers of the designed thermal actuator. Green layer is aluminum, and red layer is PI2611/10.

There are several parameters to change (as given in Eqs. (2.9), or (2.10)), in order to obtain 2 μm tip deflection. It is possible to change the length of the thermal actuator (L), thickness ratio (m), thicknesses of the bimorph actuator layers (h_1, h_2), and temperature difference between initial and final states of the materials that form the actuator (ΔT). Table 2.1 shows two different actuators that can accumulate displacement values greater than 2 μm at the tip.

Actuators / Parameters	Thermal Actuator # 1	Thermal Actuator # 2
Cantilever length (L) [μm]	100	120
Upper layer thickness (h_1) [μm]	1	1
Lower layer thickness (h_2) [μm]	2	2
Upper layer CTE (α_1) [K^{-1}]	23.1x10E-6	23.1x10E-6
Lower layer CTE (α_2) [K^{-1}]	3x10E-6	3x10E-6
Upper layer Young's Modulus (E_1) [GPa]	70	70
Lower layer Young's Modulus (E_2) [GPa]	8	8
ΔT [$°C$]*	~330	~220
Tip deflection (d) [μm] (Analytical)	-16.0	-15.4
Tip deflection (d) [μm] (FEM)	-15.3	-13.6

Table 2. 1: Parameters defining two different thermal actuators, and comparison of analytical and FEM solutions. *Temperature values are obtained from an electro-thermal analysis as explained in the next section.

These two examples of thermal actuators are analyzed both analytically and by a finite element method solver software (ANSYS®), and results are given at the end of the table. Furthermore, as a check, formulas in "Roark's Formula Book" were used in order to see whether the results are similar or not [26]. Analytical solution and "Roark's Formula Book" results matched exactly. We used the formulas given in case 6a from Table 8.1. These formulas are not for bimetallic strips, but can be modified as explained in the book in section "Composite Beams and Bimetallic Strips" in order to use for bimetallic strips.

2.3.2 Finite Element Method (FEM) solution

Finite Element Method solutions were performed using ANSYS®. Shape of the complete thermal actuator is simplified as shown in Figure 2.7, in order to reduce run-time of the solution.

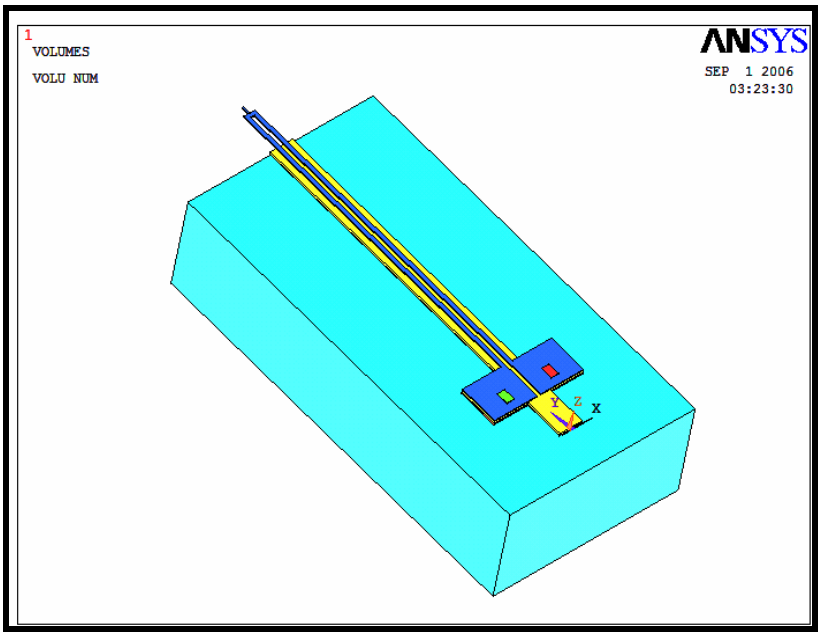

Figure 2. 6: Simplified shape of a thermal actuator

FEM solution is performed using indirect sequential method. That means, a complete solution is composed of two sequential solutions. First, the thermal actuator is heated by applying a voltage difference (Joule heating) between its two touch pads (This is the electro-thermal part of the solution.). Results obtained from electro-thermal analysis are transferred as loads to *both analytical and FEM solutions* to observe the thermo-mechanical treatments. During electro-thermal analysis, SOLID98 elements with only VOLT and TEMP degrees of freedom activated were used. In the thermo-mechanical analysis, element type is switched to SOLID92 [27], and solution is repeated in order to obtain deformed shape of the actuator.

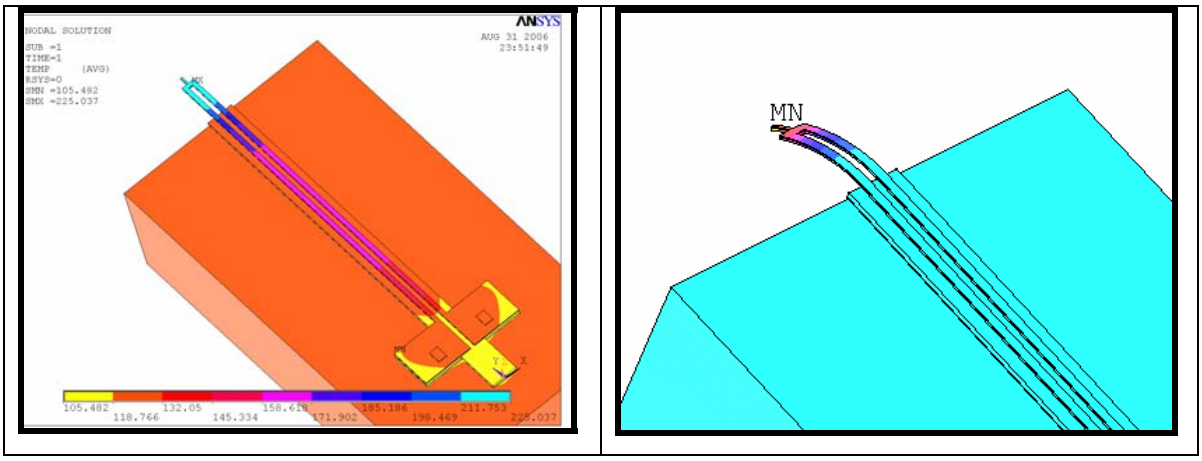

Figure 2. 7: Temperature distribution (left), and corresponding tip deflection of a thermal actuator (right).

A common mistake encountered in literature during performing the FEM solutions is to assume convection as a constant boundary layer load, which changes FEM results very seriously, and diverges the results from the real case. Natural convection heat transfer coefficient is highly temperature dependent and becomes very dominant as sizes of structures are reduced, and simply can not be avoided or can not be assumed as a constant [28, 29].

FEM solution is performed using 60 substeps for each analysis, because material properties used in the analysis were not constants, but they are temperature dependent variables. In ANSYS®, substeps are used when the material properties are highly temperature dependent and change as the solution goes on during the analysis. Similar analyses were performed previously and available in the literature [30], and [31].

2.3.3 Importance of heat transfer modes for the thermal actuation

There are three types of heat transfer modes, which are conduction, convection (natural and forced), and radiation. In the case of a thermal microactuator, heat generated by Joule heating is dissipated to the substrate by conduction, and surrounding air media by convection, and radiation. Most of the articles written previously consider only conduction to substrate as the main heat transfer mode and neglect the effects of convective and radiation heat transfer modes, or assume convective heat transfer coefficient as a constant value. However, a recently published article [31] considers all heat transfer modes, and different from the articles published previously, emphasizes the importance of natural convection and radiation. Another recently published article [30] emphasizes the importance of natural convection during the dissipation of energy to the environment. Also, it is emphasized in [28], that the free convection strongly influences heat transfer from various electronic devices (This is similar to Joule heating in our case). In addition to these, [28], and [29] emphasize that convective heat transfer is highly temperature dependent, and give the formulas to calculate it.

Free convection can be considered at 3 different surfaces of a 3D structure. These are vertical, upper, and lower surfaces of a structure. The general formulas required to calculate the average convection coefficient ($\bar{h}$) are given below. Starting with these general formulas, it is possible to calculate average convection coefficients for vertical, upper, and lower surfaces.

$$Ra_L = \frac{g\beta(T_s - T_\infty)L^3}{\nu\alpha} \tag{2.11}$$

$$\overline{Nu_L} = \frac{\bar{h}L}{k} = CRa_L^n \tag{2.12}$$

where,

Ra_L : Rayleigh Number

g : Gravity

$\beta = T_f^{-1}$: Film temperature

T_s : Surface Temperature

T_∞ : Environment (Fluid) Temperature

ν : Kinematic viscosity [m^2/s]

α : Thermal diffusivity [m^2/s]

$\overline{Nu_L}$: Nusselt Number

$\overline{h}$: Average convection coeff.

L : Length

k : Thermal conductivity

C, n : Rayleigh Number dependent Coefficient, and Exponent

For a Vertical Plate:

$$Nu_L = \left\{ 0.825 + \frac{0.387 Ra_L^{1/6}}{\left[1 + (0.492/\mathrm{Pr})^{9/16}\right]^{8/27}} \right\}^2 = \frac{\overline{h} L}{k} \qquad (\text{for } Ra_L \le \infty) \qquad (2.13)$$

For Upper Surface of a Heated Plate:

$$\overline{Nu_L} = 0.54 Ra_L^{1/4} \qquad (\text{for } 10^4 \le Ra_L \le 10^7) \qquad (2.14)$$

For Lower Surface of a Heated Plate:

$$\overline{Nu_L} = 0.27 Ra_L^{1/4} \qquad (\text{for } 10^5 \le Ra_L \le 10^{10}) \qquad (2.15)$$

Annanthasuresh *et al.* [31] emphasized that, radiation heat transfer mode becomes dominant after 500~600 K. Hence, the effects of radiation are ignored during FEM analysis that are performed during this study.

2.3.4 FEM Results and Comparison with Analytical Results

As it is shown in Table 2.1, ΔT is assumed to be an average value between the tip and the end of the thermal actuator, because the thermal actuator is long and there are temperature gradients along the direction of the electrical current flow (Figure 2.8 (left)). For convenience, finite element method analysis results are depicted in Figure 2.8 (right). As it is seen from tip deflection values for analytical and FEM solution in Table 2.2, they are quite similar, and support each other.

Actuators / Parameters	Thermal Actuator # 1	Thermal Actuator # 2
Tip deflection (d) [μm] (Analytical)	-16.0	-15.4
Tip deflection (d) [μm] (FEM)	-15.3	-13.6

Table 2. 2: Part of Table 2.1. Only analytical and FEM results are presented.

2.4 Electrostatic Actuator Design Parameters

We have chosen shape of electrostatic devices, geometric parameters of comb-fingers, and desired maximum electrostatic actuator displacement as design parameters for the electrostatic actuators. According to the information given above, it is possible to summarize them at Table 2.3 as shown below. First column defines the main shape of the electrostatic devices, and comb-finger number with the second column information defines the exact shape of the electrostatic devices. Here, the abbreviations define:

g_y: gap between two neighboring comb-fingers,

f_l: length of a single comb-finger

f_w: width of a single comb-finger

1F: Thermal actuator with one finger

3F: Thermal actuator with three fingers.

Family	Sub-Family	Comb-Finger Parameters (microns)			Desired Max Displacement (microns)		Thermal Actuator Type	
		g_y	f_l	f_w	10	25	1F	3F
X3	_3	3.8	50	5.3	☑	☒	☑	☒
	_4	1	50	7.3	☑	☒	☑	☒
	_5	3.8	81	8.3	☑	☑	☑	☑
	_6	1	81	8.3	☑	☑	☑	☑
X4	_2	3.8	81	8.3	☑	☑	☑	☑
	_3	3.8	50	5.3	☑	☒	☑	☒
	_5	1	81	8.3	☑	☑	☑	☑
	_6	1	50	7.3	☑	☒	☑	☒

Table 2. 3: Electrostatic actuator design parameters. ☑: Device designed, ☒: Device not designed.

In addition to the data presented on the table, we have chosen total number of comb-fingers, which are 50, 75 and 100 fingers, and total mechanical spring constant of a complete device as design parameters too.

If we carefully examine the mechanical spring constant calculation formula for a single spring, we see that:

$$k_{MECH} = \frac{E h_s w_s^3}{l_s^3} \tag{2.8}$$

It can easily be seen that, in a design with constant height and same material (Thus, with constant E and h_s), the only parameters of the spring that we can play with are width (w_s) and length (l_s) of the spring. Since width and length are at the same power, it is possible to write their ratio as: $\left(\frac{w_s}{l_s}\right)^3$. This explains us that, if we play with the ratio of spring width to spring length, we can have a more systematic approach for the calculation of the spring constants of the systems instead of playing with length and width of springs individually. Using this simplification in our advantage, we played with this ratio instead of playing with two variables individually. As a result, the last electrostatic actuator design parameter was $\left(\frac{w_s}{l_s}\right)$ ratio. We have chosen it as 100, 200, 300, and 400. Depending on the length of the total comb-finger array, which defines the length of the spring, we have chosen w_s, and l_s according to that, to give the final shape of the electrostatic actuators.

It is very important to emphasize that, in our designs; applied voltage was not a principal design parameter. We designed our devices such that they will give the desired displacement at about 40 to 50 Volts. However, due to the microfabrication uncertainties, we did not choose applied voltage as a principal design parameter.

2.5 Bimorph Thermal Actuator Design Parameters

As it is mentioned in section "***2.3.1 Analytical thermo-mechanic treatment***", the formula used to calculate tip deflection of a bimorph thermal actuator is:

$$d = \frac{L^2}{(h_1 + h_2)} \cdot \frac{3(1+mn)^2}{[3(1+m)^2 + (1+mn)(m^2 + 1/(mn))]} \cdot (\alpha_1 - \alpha_2) \cdot \Delta T \qquad (2.9)$$

where, d : out-of-plane tip deflection of a bimorph thermal actuator,

L : Length of thermal actuator,

m : h_1/h_2 , where h_1, h_2 represent the *lower and upper layer thicknesses respectively*,

n : E_1/E_2 , where E_1, E_2 represent elastic modules of materials used in a thermal actuator,

α_1, α_2 : Coefficient of thermal expansions (CTEs) of materials used in a thermal actuator,

ΔT : Temperature difference between initial and final states of bonded thermal actuator materials.

According to this formula, we can change only L , and ΔT as design parameters, effect of which can be observed on final thermal actuators. It is also possible to accept m , n , and α_1, α_2 as design parameters. However, because of the nature of the microfabrication, it is not possible to play with these parameters during a single microfabrication run. In other words, we can not choose m , n , and α_1, α_2 as fixed values at one specific part of the wafer, and different values at another different location of a wafer. So, m , n , and α_1, α_2 can be chosen only for once for a single microfabrication run. As it is explained above, this

rule leaves us with only two parameters to play which are L, and ΔT. ΔT is not a dimensional parameter, and can be controlled only after the fabrication of the devices. As a result we have only one parameter to change during the design of the thermal actuators, according to the formula given above.

Although it is not defined in the formula given above, there is another important parameter about obtaining a ΔT value, during actuation of the thermal actuators. It is the width of the thermal actuator layers. This parameter is specific to our actuation mechanism, because we excite our thermal actuators by Joule heating principle. Cross-section of current flowing layer, aluminum layer, is a very significant parameter according to the Joule heating principle, because of the phenomena known as electromigration.

To sum up, fundamentally we have 3 parameters to obtain different out-of-plane displacements with a bilayer thermal actuator. These parameters are, L, ΔT, and width of the thermal actuators. On the masks, we can only change width and length of the thermal actuators. Width is chosen in the range from 2 microns to 10 microns, and length of the actuators is chosen from 35 microns to 60 microns.

Thermal Actuator Design Parameters								
wire width (microns)	L (microns)	α_1 (1/K)	α_2 (1/K)	h_1 (microns)	h_2 (microns)	E_1 (GPa)	E_2 (GPa)	ΔT (Celcius)
v (2~10)	v (35~60)	f, (23.1)	f, (3)	f, (1)	f, (2)	f, (70)	f, (8)	v

Table 2. 4: Thermal actuator design parameters. f: fixed parameter, v: variable parameter

Chapter 3

EVOLUTION OF THE FABRICATION SEQUENCE

3.1 Introduction

During the optimization of the process flow for the complete integrated device, we have worked on three fabrication sequences. Each of the fabrication sequences is quite different from each other and equally possible to implement.

The main reasons for having three different process flows were:

- to use the advantage of different integration philosophies,
- to try to modify the process flows according to the availability of the equipment in the specific clean room facilities which we planned to use, and
- to find the best and easiest way to microfabricate the devices.

Names of the process flows are given below:

i. 1st Scenario: Microfabrication sequence #1
ii. 2nd Scenario: Microfabrication sequence #2
iii. Final Scenario: Process flow designed at EPFL

In this chapter, each of the flows is presented in detail.

3.2 1st Scenario: Microfabrication sequence #1

Microtweezers with two fingers have already been microfabricated at DTU [11]. The design that we worked on was closely related with the work done at [11]. [11] used two electrostatically actuated comb-finger actuators for in-plane motion, and out-of-plane motion was out of the scope of the research. In this thesis study, we aimed to increase the grabbing ability of the microtweezers by adding a thermal actuator as a third finger. This new design with three fingers is designed by considering two different actuation mechanisms integrated with each other (two electrostatically actuated fingers using in the plane of the device and a thermally actuated finger working out-of-plane).

Fabrication sequence of the 3-finger microtweezers will be presented in 2 different cross-sections as shown in Figure 3.1. Also, a color legend is drawn for reference while following fabrication steps. Detailed cross-sectional views are also shown in Figure 3.2 and Figure 3.3. Three cross-sections on the device show three critical views where attention is needed because of the complexity of the process flow. Cross-section AA shows general microfabrication sequence of the whole structure. Cross-section BB specifically shows fabrication steps of the thermal actuator parts which are constructed on polyimide (HD4100) sacrificial layer. And cross-section CC specifically shows fabrication steps followed when detaching the nanowires for the substrate surface.

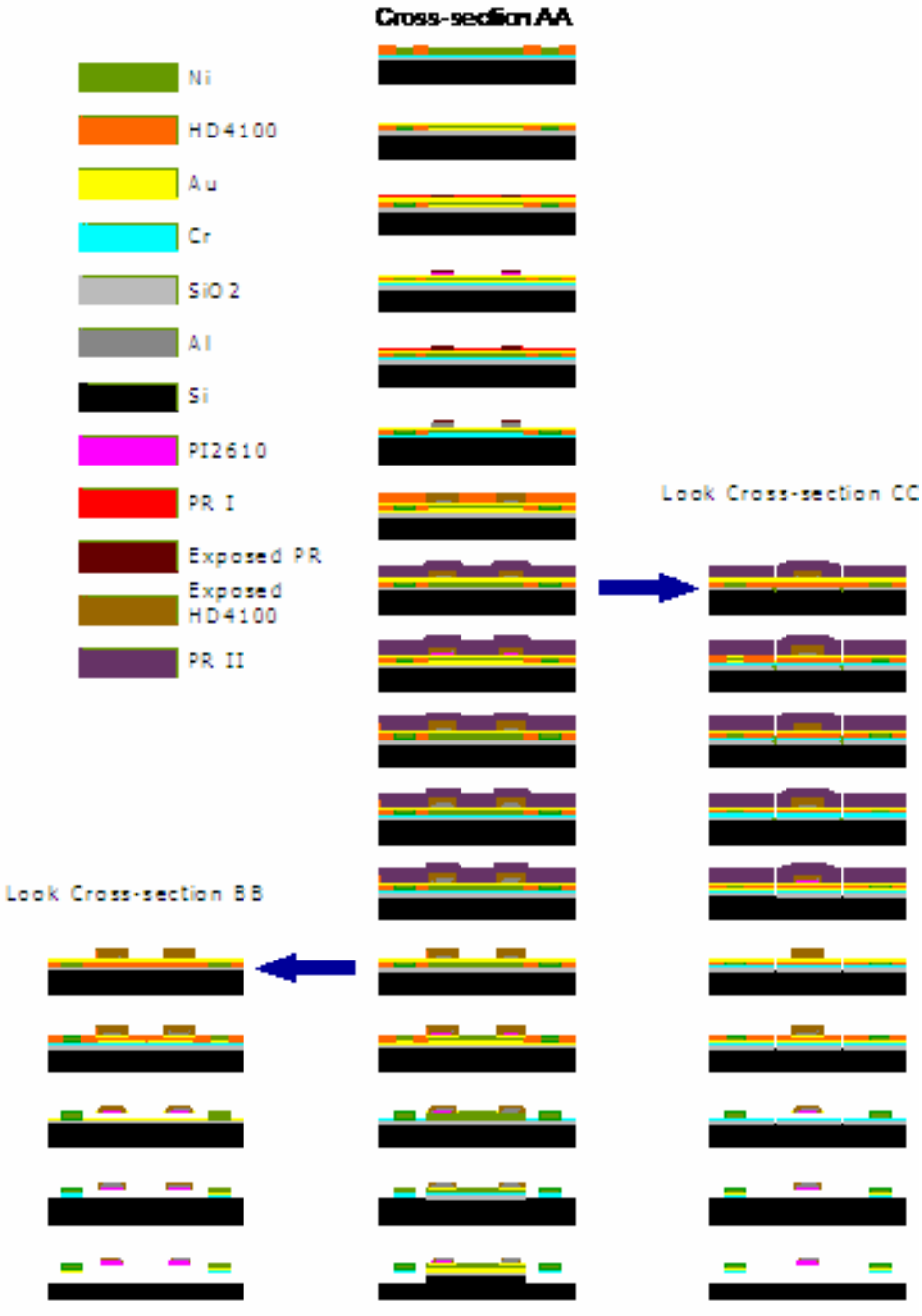

Figure 3. 1: Overview of fabrication sequence (For review purposes. Detailed pictures are shown individually.).

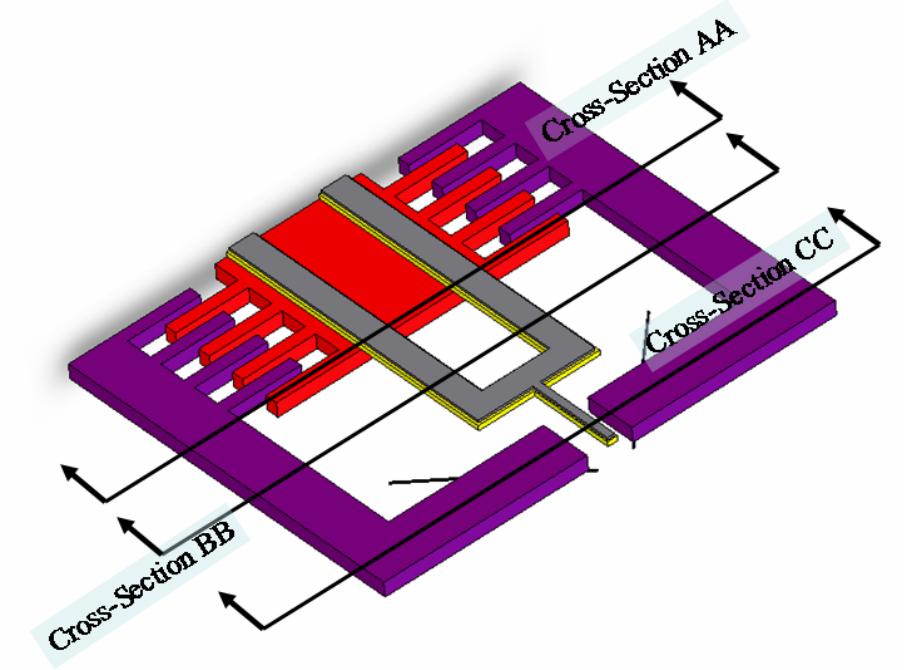

Figure 3. 2: Cross-sections AA, BB, and CC (Isometric View, Representative picture).

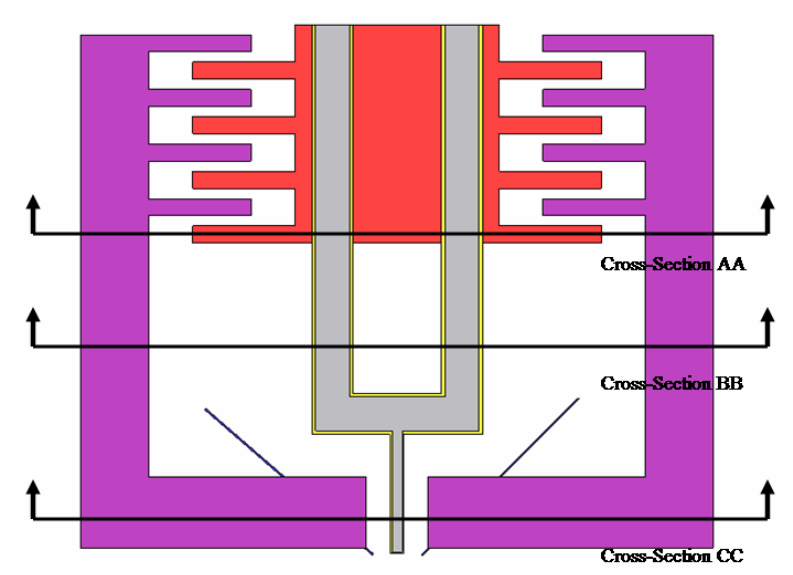

Figure 3. 3: Cross-sections AA, BB, and CC (Top View, Representative picture).

In this process scenario, molds for nanowires are obtained first. Then these molds are widened by BOE etching to etch the native oxide in the crack surface. Then these crack molds are used to fabricate the nanowires by the electrodeposition method. After obtaining the nanowires, an additional BOE step is performed to widen the cracks. After the crack widening process, Cr and Au sputtering processes are performed on the sacrificial oxide layer. This sputtering process covers the entire wafer surface and the nickel nanowires are left below sputtered Cr and Au layers. Cr layer is used as an adhesive layer between Au and oxide, while the Au layer is used as a seed layer for the fabrication of the nickel electrostatic actuator with the electrodeposition method. Using this Au seed layer, the electrodeposition of the nickel electrostatic actuators is performed. After that, thermal actuators are formed by the lift-off process. Before releasing the devices, the nanowires are detached from the other nonmoving parts on the wafer. During detaching the nanowires, other parts of the complete device are masked from the aggressive etchants present in the environment of the coming steps. The complete structure is ready for the release process after detaching the nanowires from the nonmoving parts of the structures.

3.2.1 Nanowire Formation

At first, the patterns that define the molds for nanowires are formed on bulk silicon wafer [32], [33]. Then, an oxide layer is formed with modified chemistry to form cracks as a result of proper thermal treatment. After obtaining the cracks, native oxide covers the silicon surface of the cracks very quickly. Since the silicon surfaces of the cracks are covered with native oxide, and material deposition by electrodeposition is not possible into these cracks covered with this oxide, bulk silicon wafer is immersed into BOE to etch the native oxide on the bulk silicon wafer surface. After etching of native oxide on the silicon surface, nanowires are produced by the electrodeposition method (Figure 3.4).

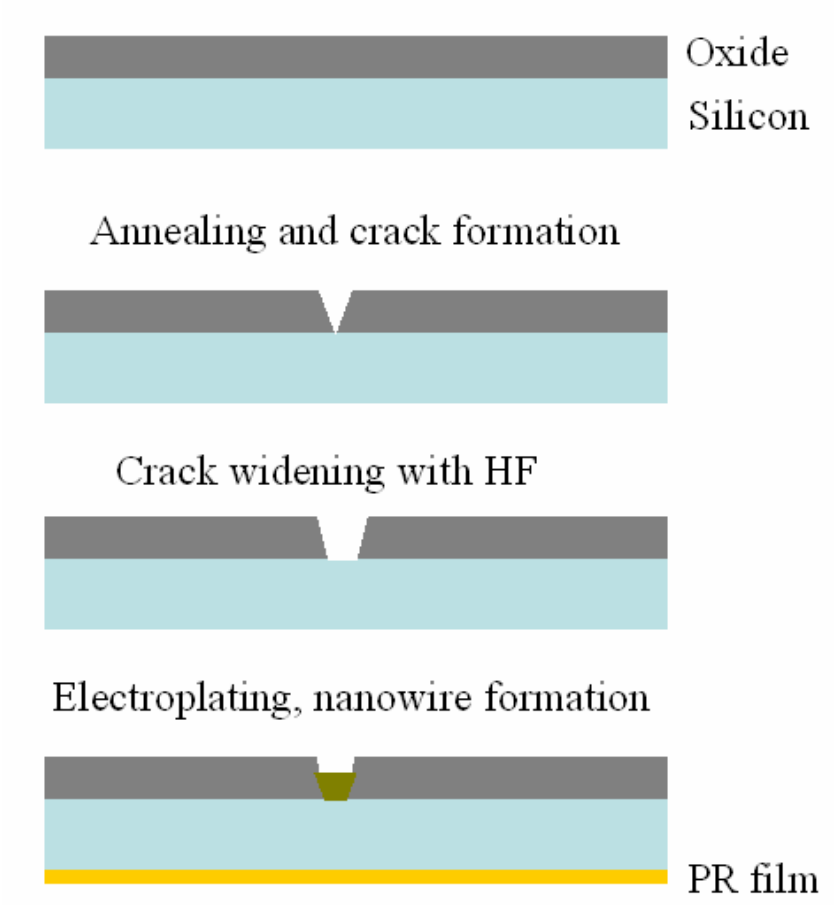

Figure 3. 4: Fabrication sequence of the nanowires.

3.2.2 Formation of the electrostatically actuated tweezers and thermal actuator

Cr and Au are sputtered on oxide as seed layer as mentioned before. Then, the conventional PL techniques are used to define the mold for the electrostatic actuators, and the electrostatic actuator is obtained. Then, first layer for the thermal actuator, known as PI2611 (HD Microsystems), is spun, and cured. The first layer of the thermal actuator is defined. Then, Aluminum is evaporated on PI, and the next PL step is performed to define the second layer of the thermal actuator (Follow the steps in Figure 3.4). Fabrication steps drawn in Figure 3.4 are from cross-section AA.

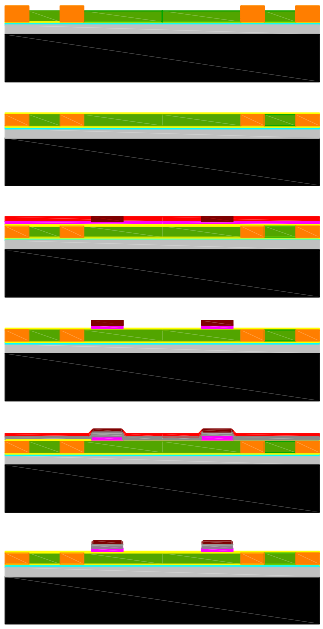

Figure 3. 5: Steps for the definition of the bimorph thermal actuators.

3.2.3 Detaching nanowires from fixed structures

At this part of the fabrication, another layer of PR is spun over the wafer, and it is defined such that there will be openings in the near neighborhood of the nanowires. These openings are used to etch the Au seed layer, Cr adhesive layer, sacrificial oxide layer, and nickel nanowires and cut them from the fixed parts of the structures (Follow the steps in Figure 3.5). Fabrication steps drawn in Figure 3.5 are from cross-section CC.

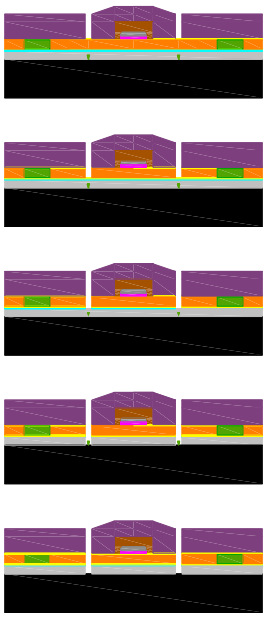

Figure 3. 6: Steps for detaching nanowires from fixed structures.

3.2.4 Release of the actuators

The last steps of the device fabrication are devoted for the release of the actuators. At first, the photoresist from the previous step is stripped. Au and Cr layers, which were used as adhesive layers for the integration of the thermal actuator with the electrostatic actuator, are etched. After this step, the PR, which was used as a mold for the electrostatic actuator electrodeposition, is removed by the oxygen ashing process. During this step, part of the PR layer, which is covering the thermal actuator, is also removed. Then, Au seed layer, Cr adhesive layer, oxide sacrificial layer are etched by their etchants respectively. Finally, the bulk silicon substrate below the movable parts of the electrostatic actuator arms is etched for deeper release (Follow the steps in Figure 3.6). Fabrication steps drawn in Figure 3.6 are from cross-section AA.

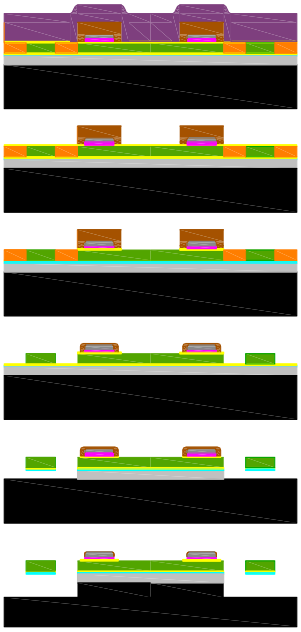

Figure 3. 7: Steps for the release of the device structures.

3.2.4 Critical issues related to 1st scenario

Reasons for selecting Aluminum, and PI2610/2611 as thermal actuator layers, HD4100 as the mold for the electrostatic actuator deposition, Au as seed layer, and Cr as the adhesive layer are given below:

a. Reasons to use HD4100, PI2610/2611 and Aluminum:

HD4100 is a kind of polyimide that has a curing temperature of about 350°C, and a degradation temperature of about 450°C. PI2610/2611 has similar curing and degradation temperatures. Because of the fabrication sequence, we have to use PI2610/2611 before removing the material, which is used as mold for the Nickel microstructure (HD4100). However, as it is explained above, curing temperature of PI2610/2611 is about 350°C, and none of the conventionally used PRs are able to withstand this temperature. As a solution, we use HD4100 instead of PR for patterning the Ni structure.

Main reasons to use PI2610/2611 as the 1st layer of the thermal actuator are: its high dielectric breakdown strength, low coefficient of thermal expansion, and high degradation temperature of about 600°C.

Aluminum is used because of its high coefficient of thermal expansion, and high electrical conductivity.

b. Freedom regarding the selection of materials:

In addition to aforementioned materials, we also have the option to use chromium, or HD4100 instead of copper as the protective layer for the upper surface, and sidewalls of the thermal actuator.

c. Etchant selectivity:

While etching unwanted parts from the structure, it is very important that *the other exposed parts be resistant to that specific etchant*. The table below is drawn for the reader to follow the compatibility of the materials with the etchants of other materials used in the fabrication process. The data presented in Table 3.1 is extracted from [34].

Because of the possibility that some questions may arise in the reader's mind, it is helpful to emphasize the points written below:

- There is no data about the effect of Cu etchants on Au. However, this is not an important consideration because the Au layer is quite thin (thickness of about 100 nanometers), and propagation of the Cr etchants in such a narrow direction is assumed to be difficult, because the etchant should struggle with the diffusion phenomena to reach the location where it needs to etch.
- One of the Cr etchants (CR-14) does not contain data about its effect on Au. This is not a big consideration because steps following the Cr etching are the removal of the Au/Cr adhesive layers.
- At the last step of the microfabrication, which is the removal of the protective Cu layer, there is no data about the effect of Cu etchant on Au, SiO_2, and silicon. However, again Au is a very thin layer embedded between two different PI layers

(HD4100 and PI2610). In addition, removal of SiO_2 and silicon (in the worst case scenario) is not an issue.

Exp.Mat. / Etchant	Cu	Cr	Al	Au	SiO_2 Annealed	SiO_2 Unannealed	Ni	Si
CR-7	280	170	3.8	0	0	0	1.7	0
CR-14	19	93	0	-	***S***	***S***	<2	***S***
HF	***S***	***S***	***W***	***S***	***W***	***W***	***S***	***S***
BHF	***R*** <5	0	11	0	490	240	<1.1	0
AU-5	***T*** 0	0	-	660	***S***	0	0	***S***
KOH	***T*** 0	4.2	12900	0	15	7.8	0	1100
Si Iso Etch	37	8.8 (***R***)	60	0	100	25	21	150
$CuFeCl_3$ 200	3900	0.053	35	-	-	-	21	-
*CuAPS*100	2500	0	<0.3	-	-	-	0	-

Table 3. 1: Compatibility of etchants with other materials used in the fabrication. Exp.Mat.: Exposed Material, Notation: **-** : experiment was not performed, ***S***: Etch rate known to be slow or zero, but etch rate not measured, ***W***: Etch known to work, but etch rate not measured, ***T***: Thicker after etch (due to swelling or compound formation) ***R***: Film was visibly roughened or attacked. Structural polyimide layer in the thermal actuator is not exposed to etchants in any step except the last Cu etching of the protective layer.

Units: nm/min.

3.3 2nd Scenario: Microfabrication sequence #2

The following process incorporates new possibilities for micro/nano integration. Islam et. al. invented a method to grow nanowires on {111} family of planes. We intended to use this method to integrate nanowires with our microtweezers. The idea behind the formation of the nanobridges between two parallel surfaces is to obtain a trench with the (111) vertical planes in the bulk silicon wafer, then to deposit a specific metal catalyst on the vertical side walls, and allow for the growth of the nanowires from one (111) plane until they reach the other (111) plane [35] (See Figure 3.7 and Figure 3.8).

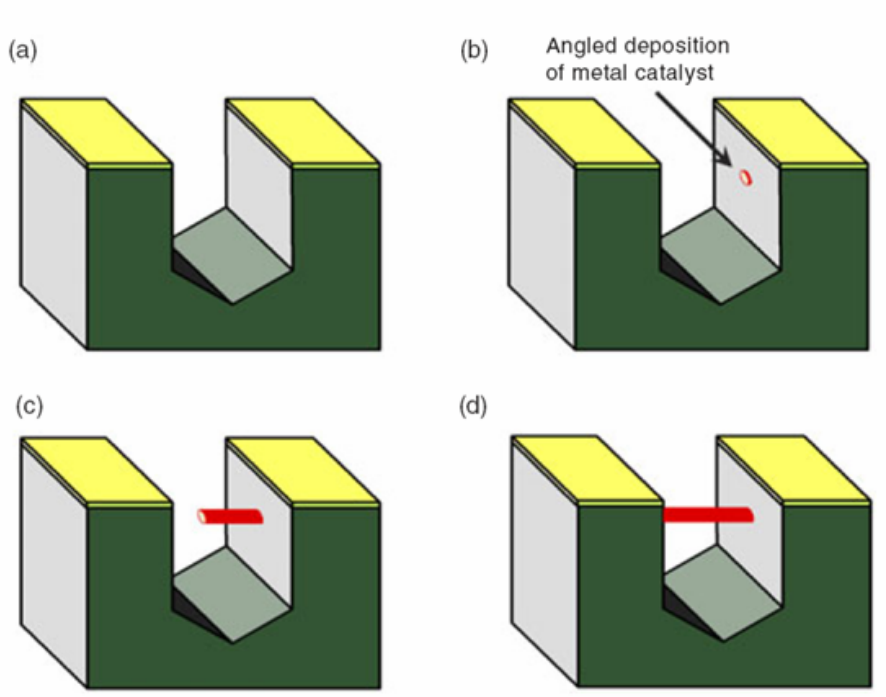

Figure 3. 8: Schematic explanation of the nanobridge fabrication method [35].

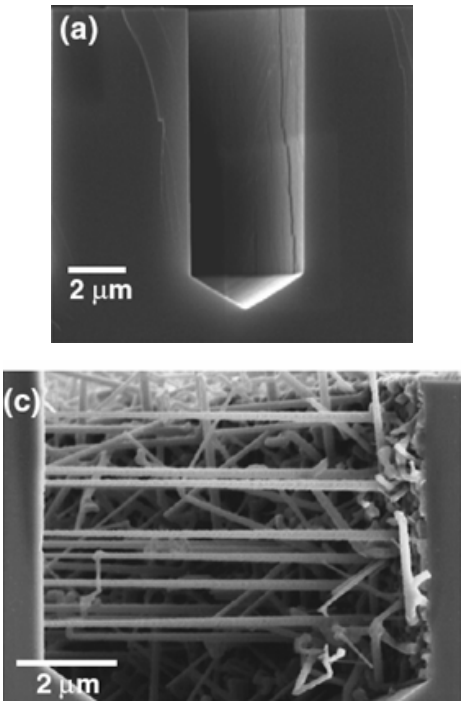

Figure 3. 9: The micrographs above show a trench in (a), where the vertical side walls are (111) planes obtained by anisotropic KOH etching of a bulk silicon wafer. In (c), nanobridges that are catalyzed with Au are shown. The trench width in (c) is 8 micron. [35]

3.3.1 Formation of Nanowires by Side Wall Deposition

In this nanobridge growth philosophy, it is important to obtain (111) sidewalls in the bulk silicon wafer. Because of this, alignment of the mask with respect to the wafer is very significant. After a successful alignment, PR is developed, and the remaining part of the PR is used as a mask for anisotropic KOH etching. After the trenches are obtained, Au catalyst is deposited on the (111) vertical planes by electron-beam evaporation at a thickness of about several nanometers. This catalyst layer is used to grow nanobridges as shown in Figure 3.8 and Figure 3.9, when the appropriate growing conditions are provided in a reaction chamber [35].

3.4 Final Scenario: Process flow designed at EPFL

In this process flow, contours (boundaries, see "4.3 Design of the "Contours of the Device Mask: Mask#1"" section of the thesis to have a better understanding of the contour definition) of the electrostatic actuator are defined with the first mask, and after that the thermal actuator is defined with the second mask. After defining both of the electrostatic and thermal actuators, third mask is used to release the actuators from their attached surfaces such that they can be actuated.

Pictures of the process flow are drawn for the cross-section shown on the Figure 3.15. However, instead of drawing exactly what is seen on cross-section AA, the drawings are simplified, as there is only one thermal actuator finger. If the cross-section AA is carefully inspected, the reader can notice that there are three thermal and two electrostatic fingers in the inset figure. In order to reduce the complexity of the fabrication sequence drawings, they are simplified, as there is only one thermal actuator finger.

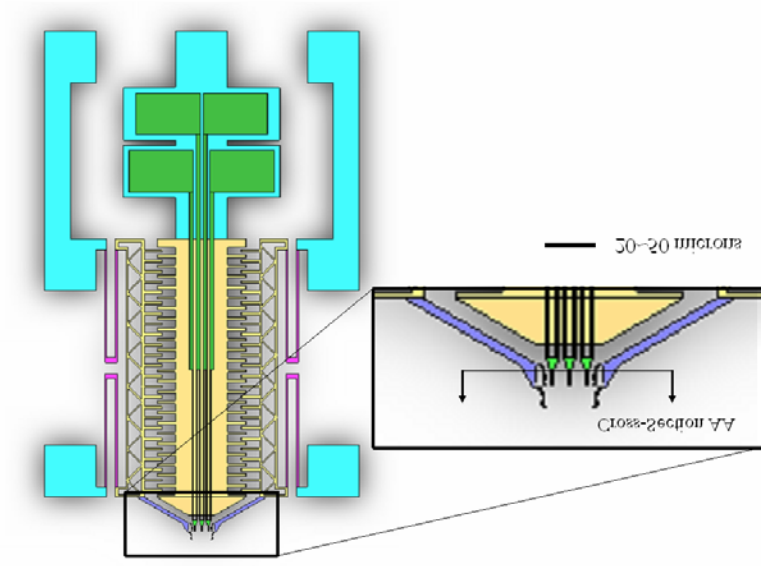

Figure 3. 10: Explanation for the location of cross-section AA with respect to device geometry.

3.4.1 Formation of the contours of the electrostatic actuator

We start with an SOI wafer, and using first mask (Mask#1), we define the contours of the electrostatic actuator as shown in Figure 3.11.

- Thermal oxide is grown as a hard mask for the first mask,
- Conventional PL steps for the definition of the contours on PR are performed,
- After the development of the PR, the oxide at the upper surface of the wafer is directionally etched until the silicon surface is reached,
- PR is stripped, and the remaining oxide is used as a hard mask for the directional etching of the upper silicon layer of SOI wafer using the recipe, which forms scalloping effect on the sidewalls of the contours.

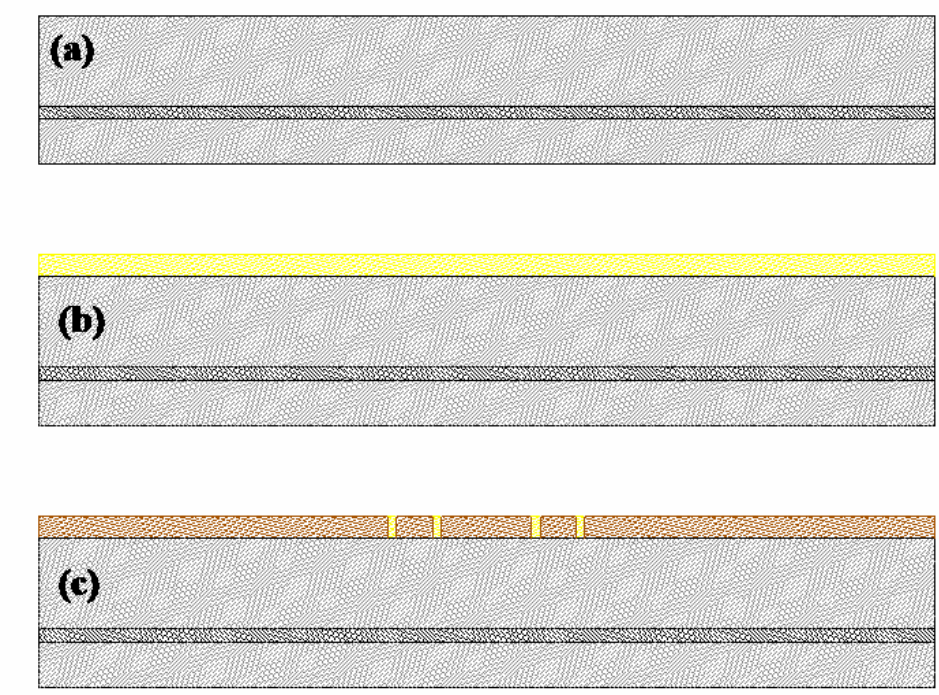

Figure 3. 11: Formation of electrostatic actuator device contours in the device layer of SOI wafer (Figure continues as Figure 3. 12).

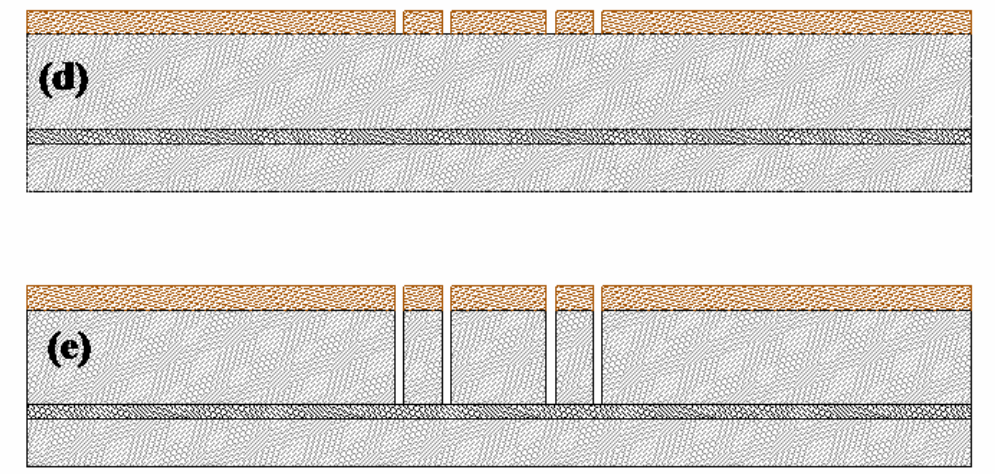

Figure 3. 12: Formation of electrostatic actuator device contours in the device layer of SOI wafer (Finished).

3.4.2 Preparation for PI Spinning and Thermal Actuator Definition

Following steps are performed to define PI2611/10 and aluminum layers and the thermal actuator itself (Figure 3.13).

- After the definition of the contours for the electrostatic actuators, our aim is to cover all the open surfaces of the wafer with thermal oxide, sputtered LTO, and BPSG with reflow at 1050 °C. We have two major reasons to use this kind of oxide formation sequence with a final reflow step:
  - ❖ In stead of forming a mechanical barrier for the isotropic Silicon etching (Such as PR spinning), we form a thin chemical barrier which will do the same thing as a mechanical stop does, and furthermore is able to reduce the surface topology for the coming steps of the process,
  - ❖ If the reflow step is not done, PI, which is going to be spun at the next step, flows from the small gaps till it stops by itself. However, this process is not controllable and affects the results of the coming steps and as a solution we decided to do a final reflow step at 1050 C and close these small gaps with reflow.

- After the oxide layer formation on the surface of SOI wafer, we spin PI and perform the curing process for PI as it is stated in [36] (This is the base layer of the thermal actuator).
- Aluminum evaporation is performed (This is the top layer of the thermal actuator).
- Conventional PL steps are utilized to define the mask for the formation of the thermal actuator
- Aluminum, PI, and oxide directional etching is performed respectively.

At this point, the definition of the thermal actuator is completed and the only remaining step for the actuation of the thermal actuator is the complete release of the movable parts of the device.

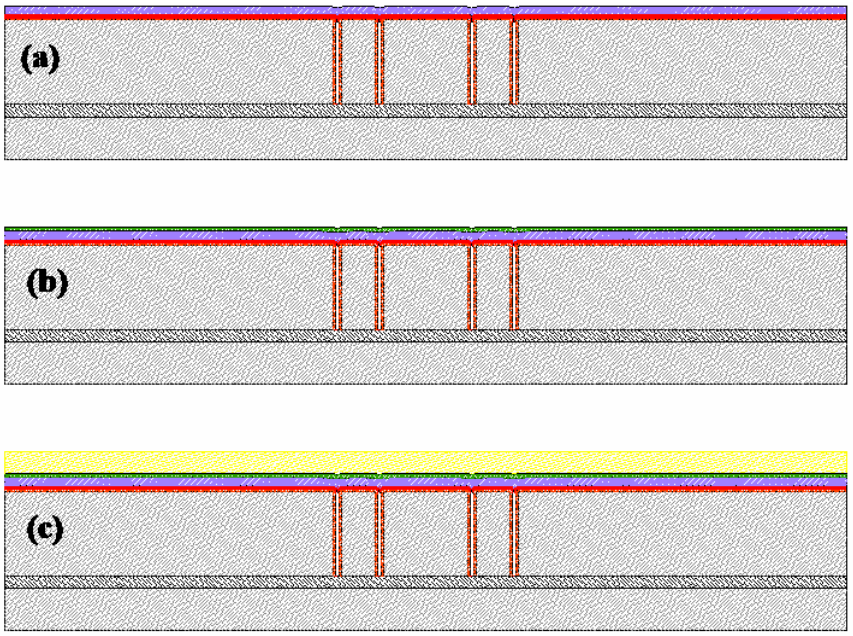

Figure 3. 13: Steps required for the formation of the thermal actuator (Figure continues as Figure 3.14)

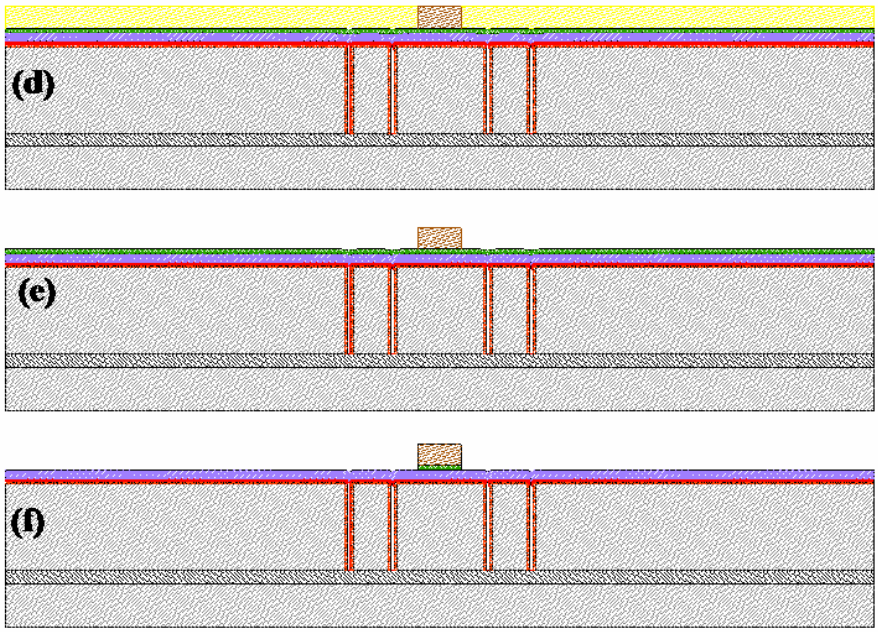

Figure 3. 14: Steps required for the formation of the thermal actuator (Figure continues as Figure 3.15)

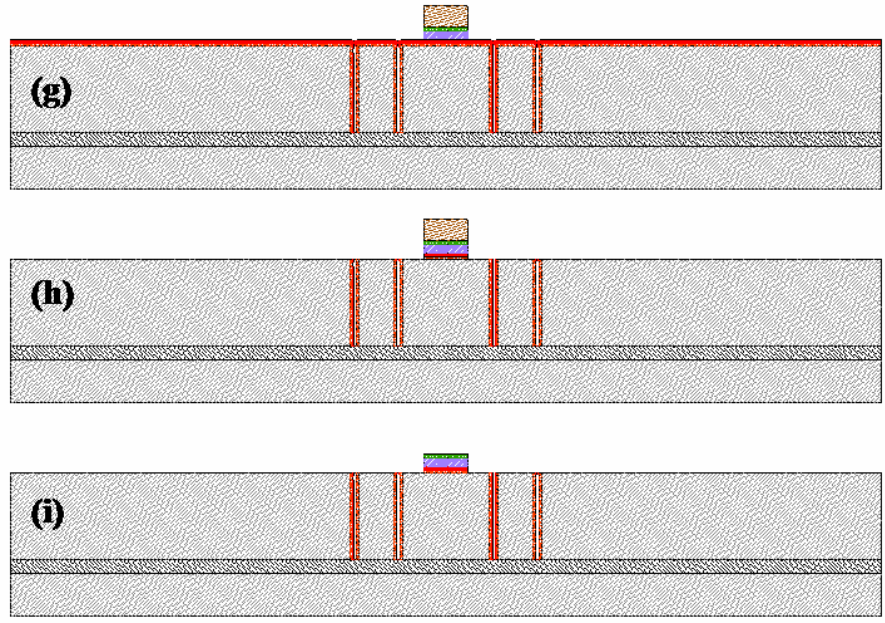

Figure 3. 15: Steps required for the formation of the thermal actuator (Finished).

3.4.3 The Release of the integrated structure

Although we call these steps as the release of the complete device, they are also used to completely define the electrostatic actuator (Figure 3.16).

- First, the conventional PL steps are performed to define the mask,
- Isotropic Silicon etch is performed. After this step, the electrostatic actuator is completely defined but it is still not completely released from the buried oxide layer of an SOI wafer.
- Directional oxide etch and isotropic oxide etch are the following steps to release the device from buried oxide layer.
- The final step is the stripping of the PR.

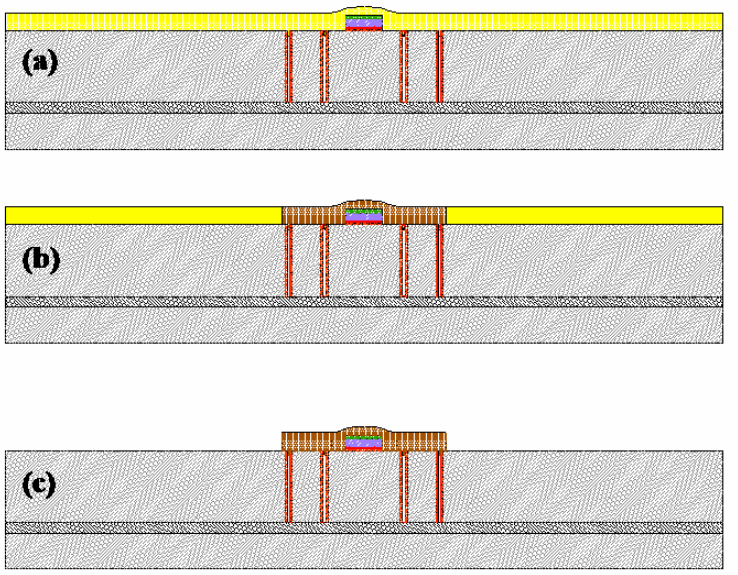

Figure 3. 16: Steps required for the release of the device (Figure continues as Figure 3.17)

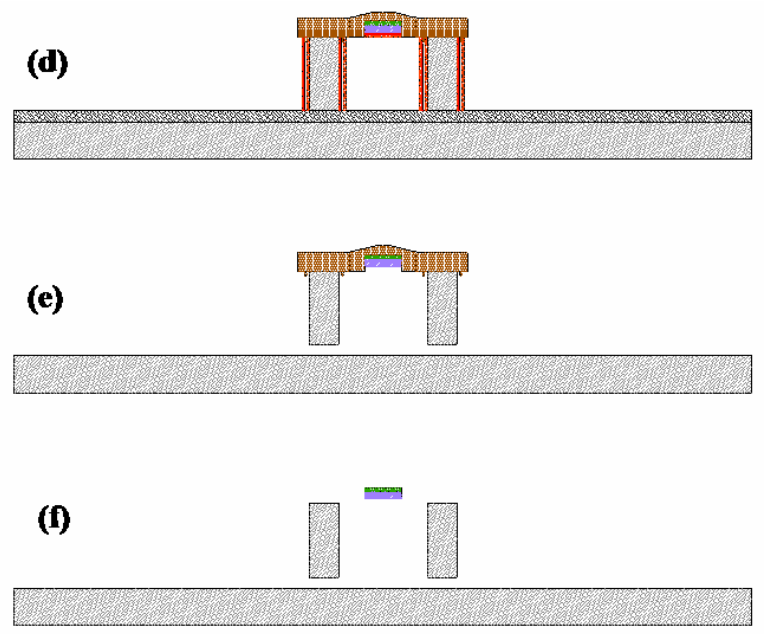

Figure 3. 17: Steps required for the release of the device (Finished).

Chapter 4

LAYOUT DESIGN AND THE OPTIMIZATION OF THE LAYOUT

4.1 Introduction

According to the final fabrication sequence, designed at EPFL, there are 3 masks in the process flow. These masks are named as “Contours of the Device Mask: Mask#1”, “Thermal Actuator Mask: Mask#2”, and “Release Mask: Mask#3”.

During the design of the masks, we started with the first generation of the electrostatic and thermal devices. In this first trial, we worked with bulk silicon wafers, although our real process flow was not appropriate for bulk silicon wafer microfabrication. The reason for the production of these first generation masks on bulk silicon wafers was to understand how the designed process flow would work, to see possible major problems that we can encounter during fabrication, and to reduce the cost of consumables. After addressing the issues with process flow and performing the optimizations, we switched the process to SOI wafers in order to obtain functional electrostatic devices.

Basically, the questions in our mind during designing the process flow before the microfabrication results are obtained were:

- Will we be able to draw contour lines of 1-micron width on the Cr masks? At the beginning of the process we were informed that it could be difficult to obtain 1-micron contour widths on the mask, and as a result we decided to use two different contour widths of 1 micron and 2 microns.
- How will the Photoresist (PR) thickness affect the remaining phases of the process?
- How will the grown oxide profile change through the depth of the silicon wafer?
- How uniform will be the oxide profile in the complete silicon wafer?

- What surface topologies will we have after the oxidation, and how will it affect the next steps?
- How will we solve the alignment problems?

After the first generation of the masks and devices, we saw that the process flow is appropriate for the production with minor changes in the process flow. These minor changes are discussed in 5th chapter of this work.

After the first trial on bulk silicon wafers and addressing the possible issues related to the fabrication sequence and layout design, we switched the process for the second generation of the devices to SOI wafers.

4.2 Map of the complete devices on the Cr Masks

In order to investigate the limits of the applicable devices, our design workspace covers a wide range of device geometries with different comb-finger numbers, geometry and displacement ranges, mechanical spring geometry, thermal actuator lengths, thermal actuator shapes, and thermal actuator finger numbers.

Device shapes can be classified under two main families. This classification is done according to the shapes of the electrostatic devices, and those main families are shown in Figure 4.1. Furthermore, we worked on four different types of sub-families for the electrostatic actuators. Families are defined according to the main shape of the devices and the sub-families are defined according to major changes in the shape of the comb-finger geometries (Figure 4.2).

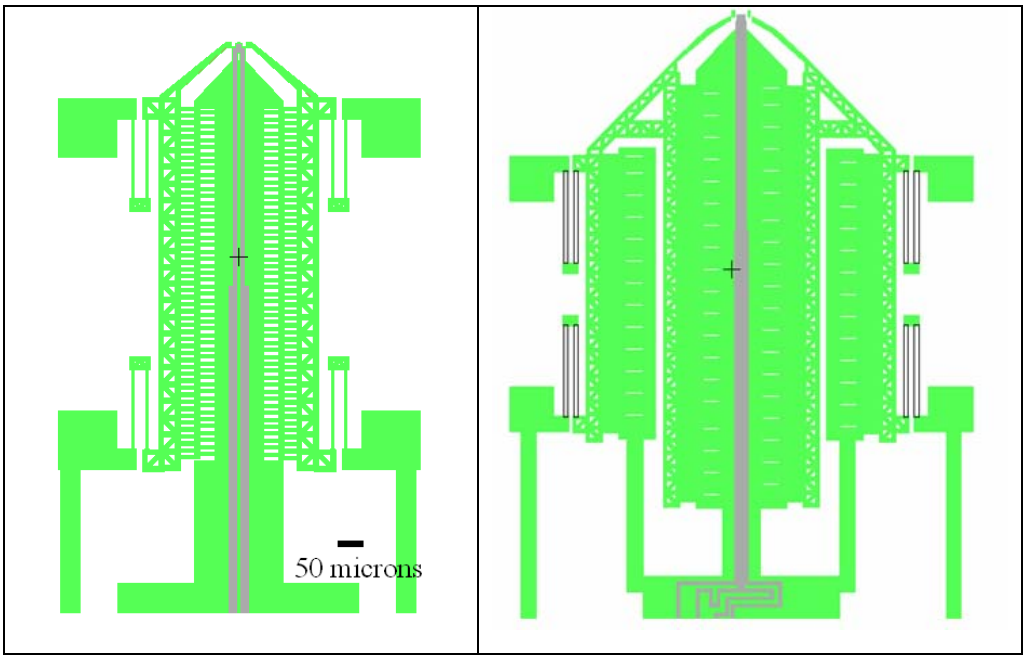

Figure 4. 1: Two types of families of devices used in the design

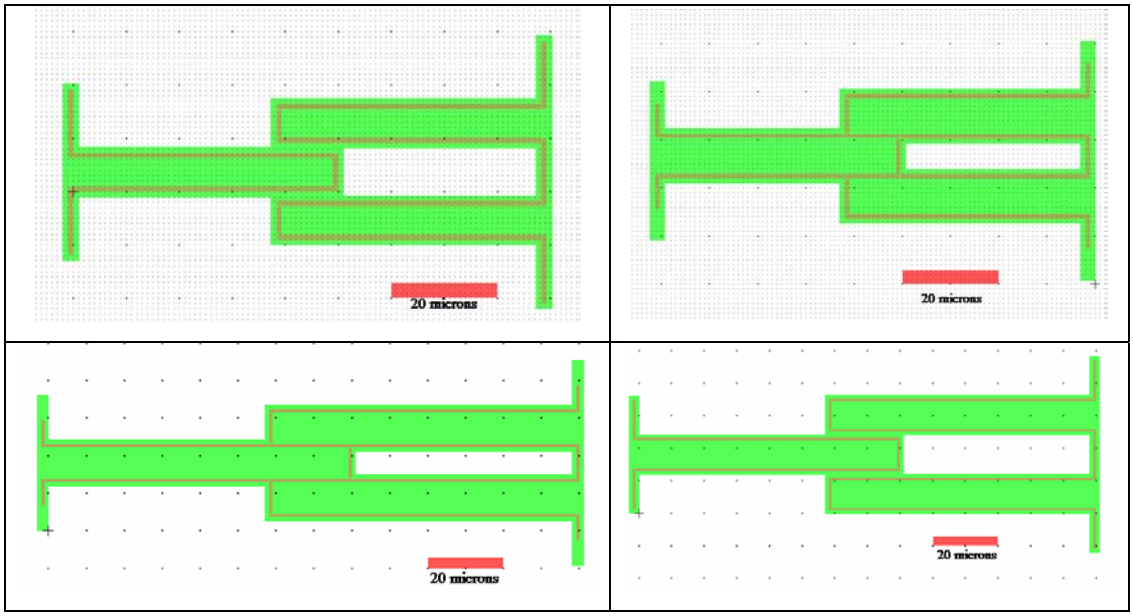

Figure 4. 2 : Four types of comb-finger geometries

According to the device classification we have two main groups of devices in the masks and wafers. These devices are:

1. Devices that contain thermal actuators, electrostatic actuators and integrated nanowires,
2. Devices that contain only electrostatic actuators and integrated nanowires, but no thermal actuators.

		Contain a thermal actuator	Not contain a thermal actuator		
Family Type	X3	☑	☑	CF1	Comb-Finger Types
		☑	☑	CF2	
		☑	☑	CF3	
		☑	☑	CF4	
	X4	☑	☒	CF1	
		☑	☒	CF2	
		☑	☒	CF3	
		☑	☒	CF4	

Table 4. 1: Types of devices on the masks and wafers. X3 and X4 represent the families. CF1, CF2, CF3, CF4 represent the comb-finger types shown in Figure 4.2.
☑: drawn on the masks, ☒: not drawn on the masks.

We also have a total of 21 types of thermal actuators, 15 of them are for single thermal finger actuators (Figure 4.3 (left)), and the remaining 6 types are for 3 finger thermal actuators (Figure 4.3 (right)). Since the thermal actuators are randomly distributed in the devices they are not classified in this table. However, it is significant to say that, this random distribution is not a completely random distribution, and according to the experience from the first generation devices, number of most robust devices is greater than

the thermal actuators with low possibility of survival in the end of the complete microfabrication process.

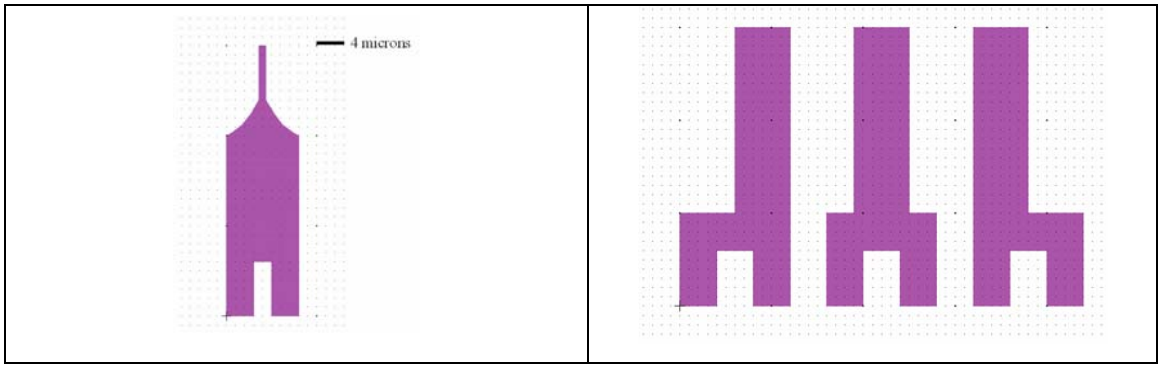

Figure 4. 3: Two types of thermal actuator families. An actuator with one thermal finger (left), and actuators with three thermal fingers (right).

4.3 Design of the "Contours of the Device Mask: Mask#1"

This mask is the 1st mask of the process. It defines the boundaries of the electrostatic devices on the SOI wafers (Figure 4.4). After the optimization of the process flow, we decided to use a contour width of 1 micron for the boundaries of the electrostatic devices (As we informed the reader about the contour width selection for the first mask definition on the wafers, we started the fabrication of the devices with two different contour widths. These were 2 microns and 1-micron contour widths. After the microfabrication results of the first generation devices we decided to use 1-micron contour width.).

The design rule we followed when forming the first mask was to draw a pseudo device at the beginning. Then the boundaries of the device were defined visually and the contours were drawn using this pseudo device as key features (See Figure 4.5 to understand easily with a demonstration). The main reason to choose this way was to draw the contours of the devices easily. Also, assuming that there was no device geometry on the mask to define its

contours, the mask drawing process became relatively very difficult because there is no device geometry that we can use to draw the contours appropriately.

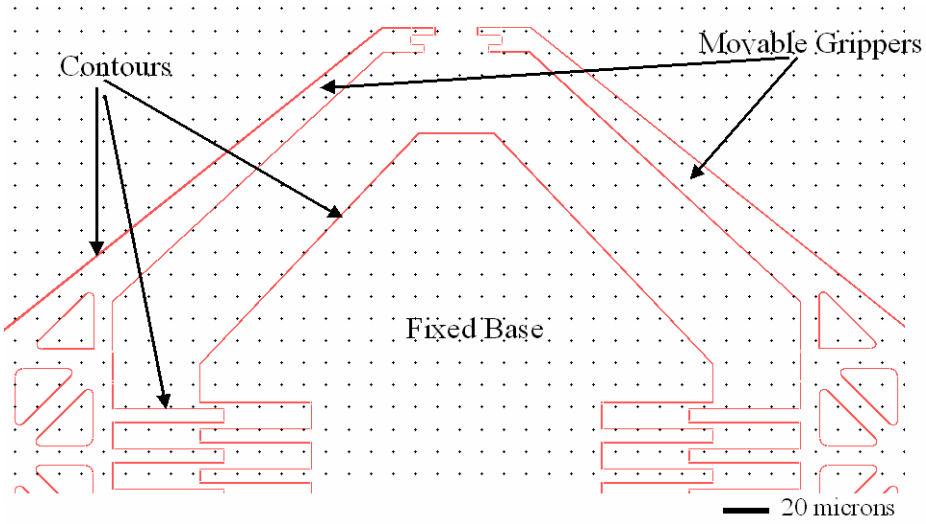

Figure 4. 4: First mask of the process flow. Red lines on the figure represent the contours.

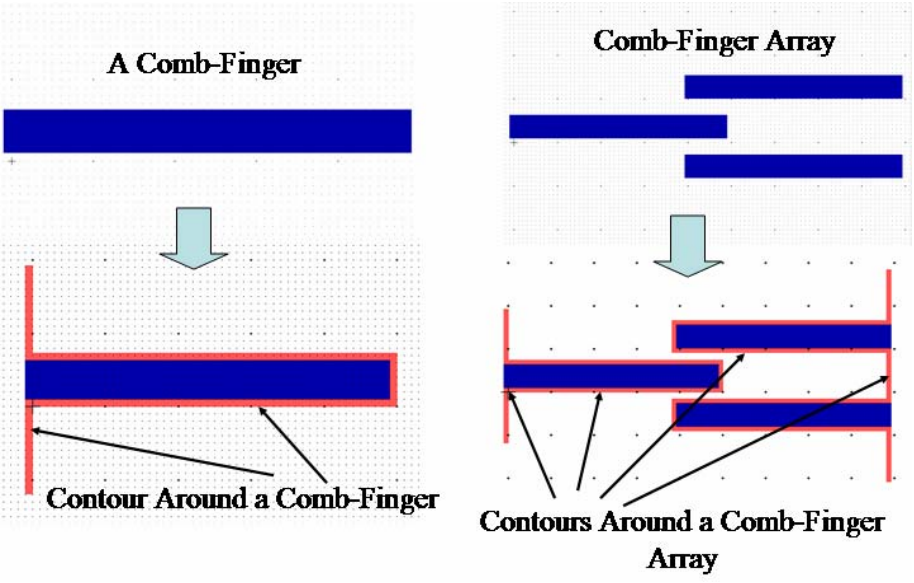

Figure 4. 5: A demonstration to explain how the device contours were drawn on the mask.

4.4 Design of the "Thermal Actuator Mask: Mask#2"

In the design of the thermal actuator mask, we used the conventional method to draw the thermal actuators (Conventional means, we used the exact shape of the thermal actuators to draw the mask instead of using the method that we used to draw contours of the devices on the first mask.). We used mainly two different thermal actuator types. First one has only one thermal finger (Figure 4.6), and the second one has three thermal fingers (Figure 4.7).

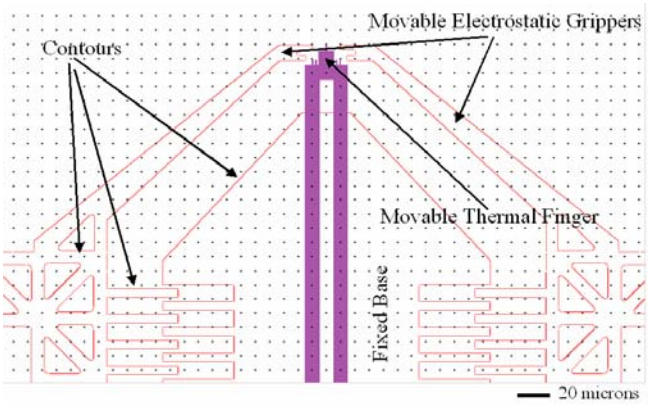

Figure 4. 6: A thermal actuator with one thermal finger

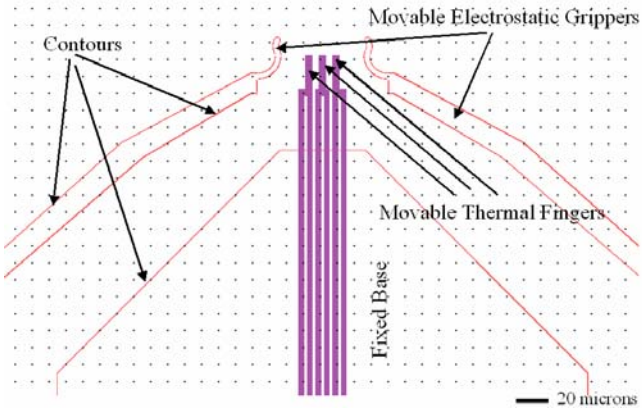

Figure 4. 7: A thermal actuator with three thermal fingers

4.5 Design of the "Release Mask: Mask#3"

The aim of the release mask was to cover the whole top surface of the complete device (thermal actuators, electrostatic actuators, nanowires and touch pads) and act as an etch stop layer to prevent the device from the aggressive environment which includes isotropic silicon etchant and isotropic oxide etchant (Figure 4.8). The sidewalls of the electrostatic devices are covered with oxide, and this sidewall cover acts as an etch mask layer for the isotropic silicon etchant. At the next etching step, which is the isotropic oxide etch, the cover at the side walls is also etched with the oxide etchant, after completing its mission at the isotropic silicon etch step.

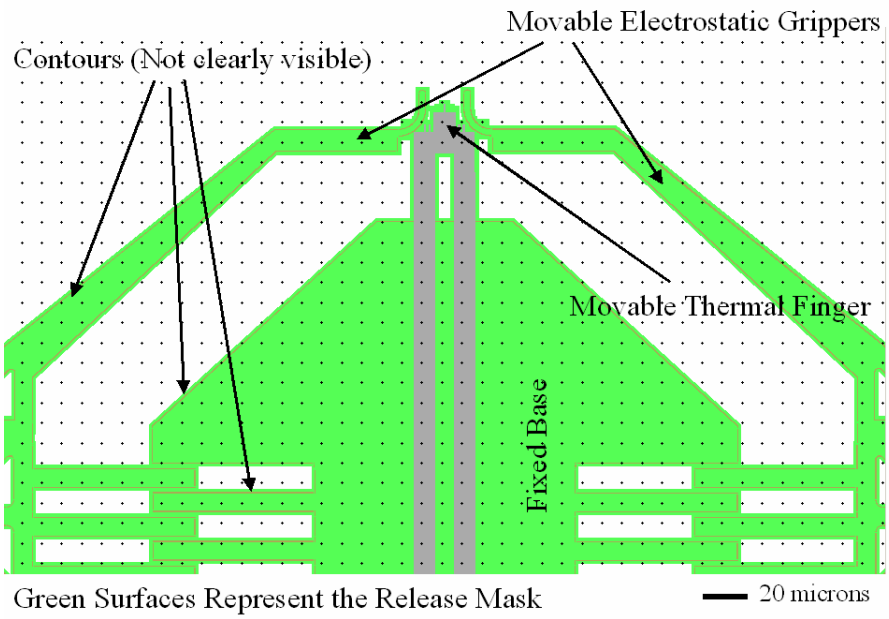

Figure 4. 8: Shape of the release mask. Green colored surface represents the surface covered by the release mask photoresist. Top surfaces of both electrostatic actuator and thermal actuator are covered. Also, the nanowires at the tip of the electrostatic actuator are below the release mask during isotropic etching processes.

4.6 Test Structures on First Mask

Test structures are drawn only in the first mask in order to optimize the photoresist parameters according to our purposes. However, we also utilized them in the second and third masks to see the final results. Also, since we aimed to obtain nanowires integrated with the electrostatic actuators, we used test structures to observe the minimum nanowire width that we can obtain with the microfabrication technology we developed (Figure 4.8, Figure 4.9).

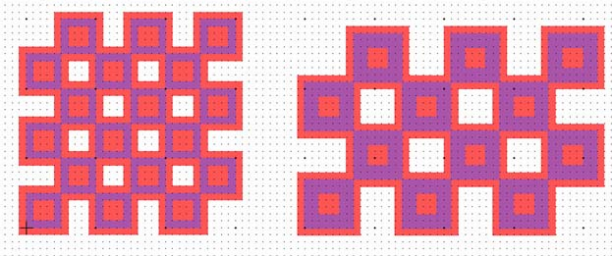

Figure 4. 9: Chess table structures for PR thickness, UV exposure optimization, and development of the PR process.

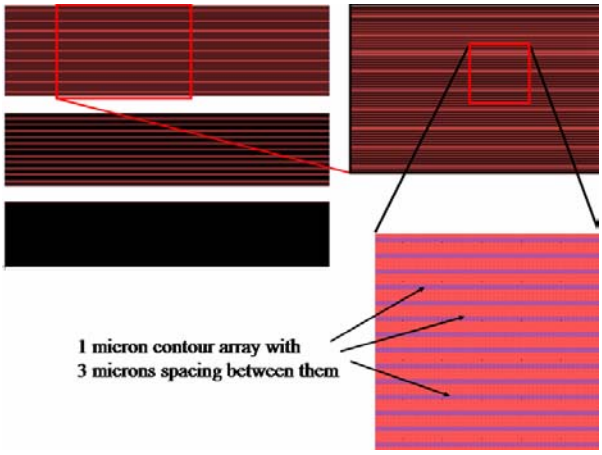

Figure 4. 10: Structures used to optimize radii of the nanowires for the integration process.

4.7 Touch Pads for Electrostatic and Thermal Actuators

Although the touch pads seem as insignificant, they cover the biggest area in a die. It was important to fabricate touch pads of thermal actuators on top of electrostatic actuator touch pads, because the last step of the process flow was for the release of the devices by isotropic silicon and oxide etching. If the places for the touch pads of the thermal actuators were not correctly located, they would not be able survive from isotropic silicon etching. In order to prevent this issue, we reserved certain area for thermal actuator touch pads on the central touch pads of the electrostatic devices, and constructed the thermal actuator touch pads on these central electrostatic touch pads (Figure 4.10).

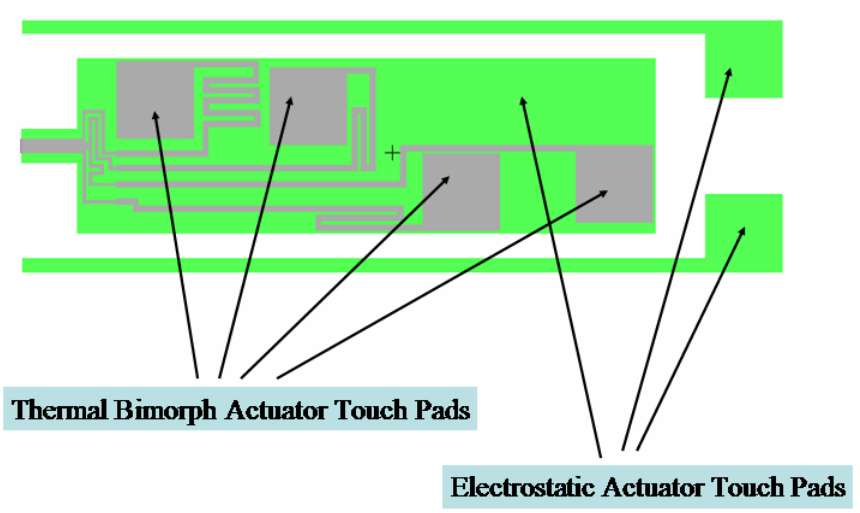

Figure 4. 11: Thermal actuator touch pads were located on the central touch pads of electrostatic actuators. Green parts on the figure represent the area that survives after isotropic silicon and oxide etching, and touch pads are below the central green part in the figure.

4.8 Complete Mask

Complete mask is composed of dice, alignment marks, and names of the masks as shown in Figure 4.11. Mask names are intentionally drawn out of the active workspace of the silicon wafers, since they are not required on the wafer, and the main reason to draw them on the Cr masks is to easily identify the masks in order to save time before the UV exposure. Simply, these names are used to be sure without inspection the masks under a microscope.

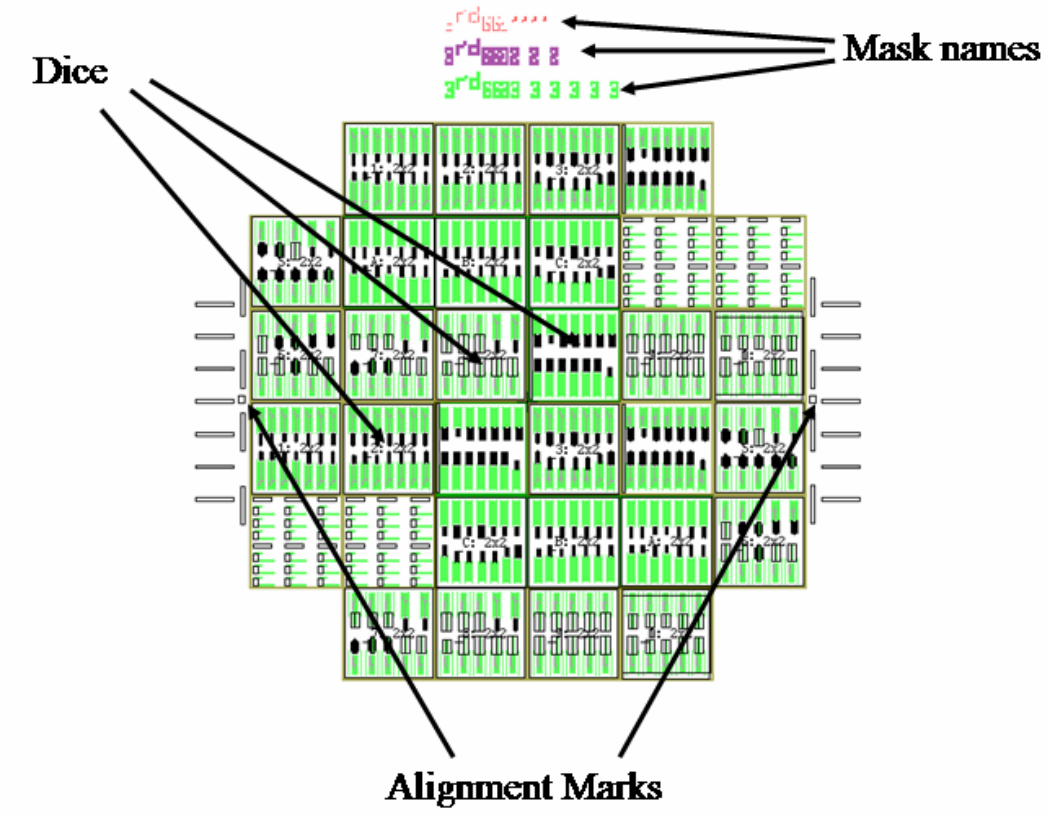

Figure 4. 12: Complete layout which was patterned on 5 inches of Cr masks.

Chapter 5

TECHNOLOGY DEVELOPMENT AND DEVICE FABRICATION

5.1 Introduction

This chapter is dedicated to present the studies about how we managed to optimize the parameters according to our purposes. According to the suggestions from a photolithography expert of CMI (Center of MicroNano Technology), the best way to obtain the devices with the desired geometries was to make photolithographic corrections on the masks by modifying them as second generation and third generation masks. This was the conventional method to obtain the desired geometry for the devices. Because of the way we followed during the development of the devices, we can divide this chapter into two main sub-titles, which are optimization based and characterization based fabrication of the devices.

5.2 Optimization Based Fabrication (First Generation)

In optimization-based fabrication, we used bulk silicon wafers instead of SOI wafers in order to reduce the cost of the fabrication. In the end of the fabrication of first generation devices, we were planning to see if we would be able to geometrically define the electrostatic actuators and thermal actuators on top of the electrostatic actuators. In other words, we aimed to find an answer to the question of device integration. Also, this was a good opportunity to see what kind of unexpected problems will be encountered during the fabrication.

5.2.1 Photoresist (PR) Thickness and Photolithography Corrections

On the first mask#1, there were 4 different photolithographic considerations of the same device. They were:

1. Device with the original geometry transferred to the masks using 1-micron contour width,

2. Device with corrected geometry according to the first suggestions from the stuff of CMI, using 1-micron contour width (Devices with photolithographic correction),

3. Device with the original geometry transferred to the masks using 2 micron contour width, and

4. Device with corrected geometry according to the first suggestions from the stuff of CMI, using 2-micron contour width (Devices with photolithographic correction).

According to the obtained results, PR (AZ9260) thickness and developed PR profile was not appropriate to etch silicon layer for our purposes, as a solution we decided to use another thinner PR (AZ92xx, diluted version of AZ9260), and a hard mask (oxide) in the second generation of the devices. The thin layer of PR was used in order to define the hard mask (oxide), and the hard mask was used instead of a PR layer as a mask to define the structures on silicon layer (Figure 5.1).

5.2.2 Comb-finger Profile

We planned to use SOI wafers with 50 micron and 10 micron device thickness for the final generation of the devices. In the first generation devices, we investigated how the comb-finger profile changes as a function of device thickness layer depth in bulk silicon wafers (Figure 5.2, and Figure 5.3).

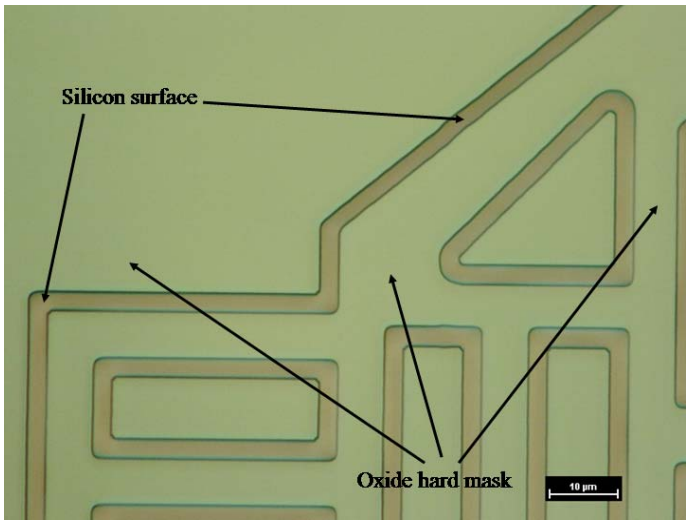

Figure 5. 1: This optical microscope picture is taken after PR is stripped from the surface of the wafer. The oxide remaining on the wafer is used as a hard mask to etch silicon trenches. After the directional silicon etching using the SOI_Sharp recipe of CMI [37], the oxide mask is etched away.

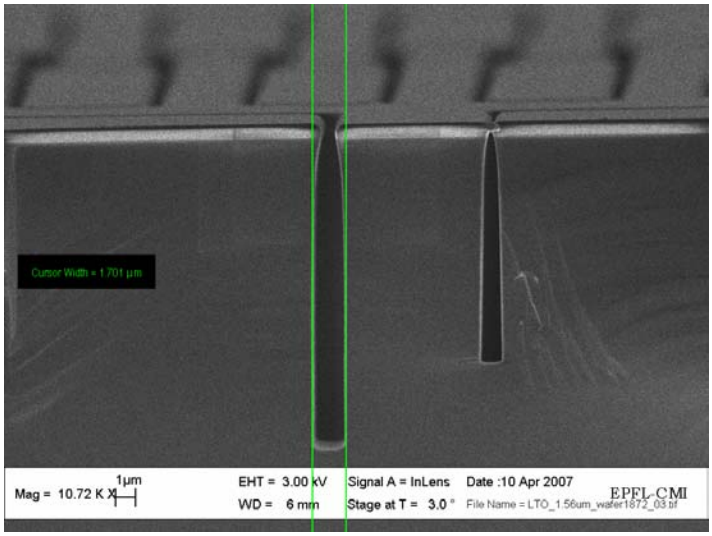

Figure 5. 2: Due to different contour widths, the *loading effect* is easily seen on the wafer. This is an undesired result because of using different contour widths on the same device.

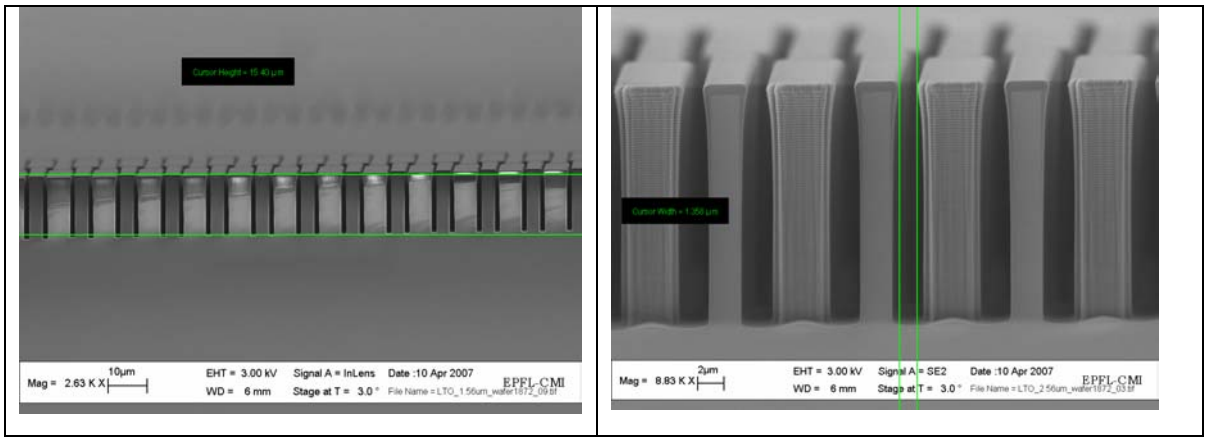

Figure 5. 3: These micrographs (right and left) show the profiles of the comb-fingers in the bulk silicon wafer. Recipe used to obtain these profiles is SOI_sharp of CMI [37]. The profile obtained by this recipe is appropriate for our purposes.

We also investigated how the comb-finger profile will change when we expose the wafers to thermal oxidation in order to close the gaps of the contours. This topic is explained in the next section.

5.2.3 Oxide Profile to Close the Contour Gaps

We optimized the oxide thickness and oxide treatment recipe such that the next step material (PI2611) will not leak into the nanometric scaled gaps because of the contour line widths. We tried four ideas to achieve our purpose. These were:

1. Using only thermal oxidation to close the trench width gaps (Figure 5.4),
2. Using only LTO to close the trench width gaps (Figure 5.5),
3. Using a combination of thermal oxidation and following the thermal oxidation by an LTO layer deposition (Figure 5.6), and finally,
4. Using thermal oxidation, LTO deposition, BPSG deposition and reflow of the deposited oxides at 1050 C° (Figure 5.7).

The main difference between the 1st and the 2nd ideas were the surface quality and the final trench width after the oxide growth or oxide deposition. Thermally grown oxide gave a good trench sealing, while the surface quality of the wafer at the contour regions after this process was rough for the coming steps. Deposited LTO gave a good surface quality, however the contour trenches were not completely sealed. As a lesson from these two trials, a combination of thermal oxide growth and LTO deposition, which gave a better surface quality and gap sealing, was used as a third trial. However, the results were still not completely satisfying (Figure 5.6, and Figure 5.7). Because of this, we tried the 4th idea to obtain the surface quality we want (Figure 5.8). The figure obtained after the 4th idea shows the effect of BPSG deposition and reflow of the oxides at 1050 C°, which blocks slipping of PI and next photolithographic step photoresists into the gaps of the contours.

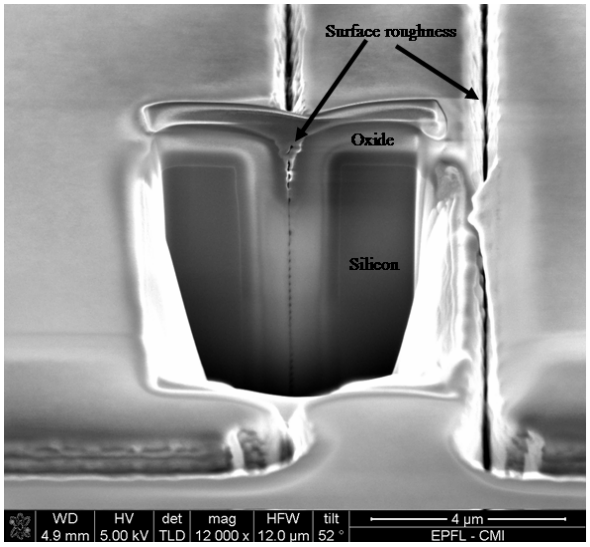

Figure 5. 4: The aim of this process recipe was to seal the contour gaps by exposing the wafer to thermal oxidation. Due to a thin gap between the final two oxide walls, this recipe was not use to seal the contour gaps.

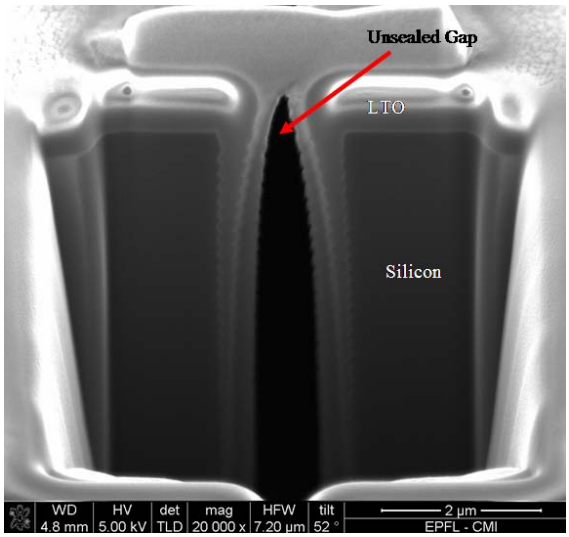

Figure 5. 5: Deposited LTO gave a better surface quality, however the gaps due to the contours were not sealed after LTO deposition to the silicon surface and contour lines of the electrostatic actuators.

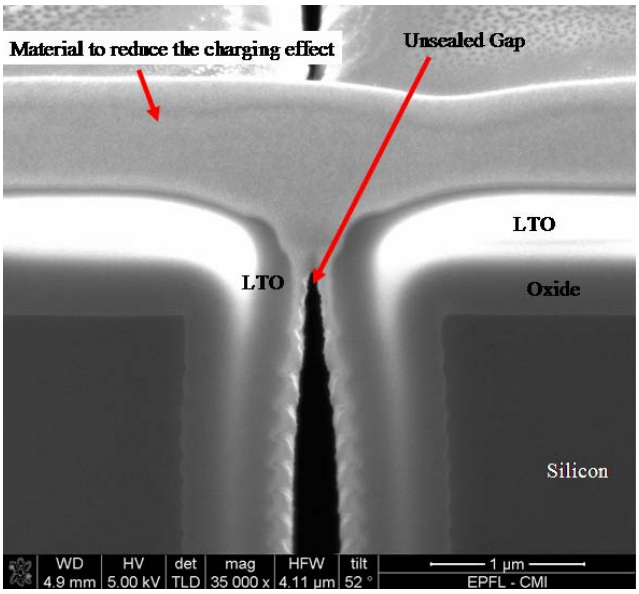

Figure 5. 6: A combination of thermal oxidation and LTO deposition on the silicon surface. The gap is not completely sealed.

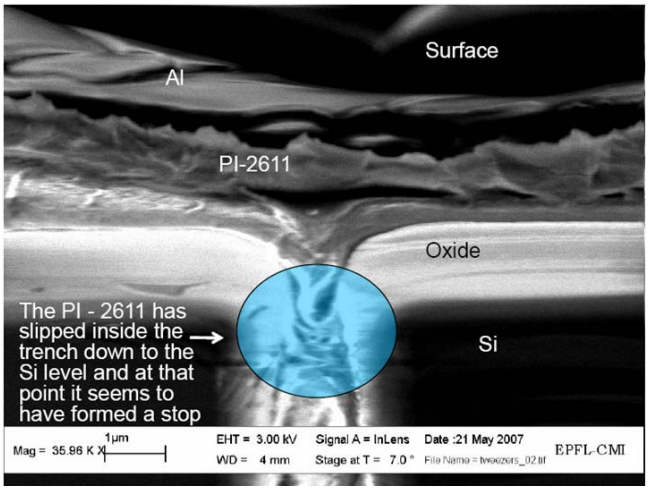

Figure 5. 7: Leakage of PI2611/10 into the unsealed contour gap.

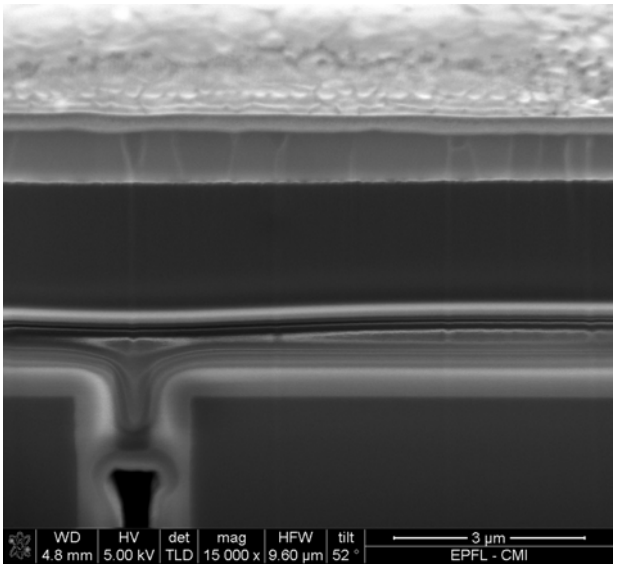

Figure 5. 8: Result after the fourth recipe. Thermal oxidation, LTO and BPSG deposition was followed by reflowing process at 1050 C°. The obtained surface quality and the gap sealing were appropriate for the purposes of the process sequence.

5.2.4 Thermal Actuators

Next step after PI coating, curing and aluminum evaporation was the second lithography in order to define the shapes of the thermal actuators. AZ92xx, which is a diluted version of AZ9260, was defined with the "Thermal Actuator Mask: Mask#2". After the development of the PR, it was used as a mask to anisotropically etch the aluminum on PI layer. As a result of this etching, the upper layer of thermal actuators was defined. After that, the remaining PR and aluminum layer below the PR were used as a mask in order to anisotropically etch the PI to define the second layer of the bimorph thermal actuators. After all these steps, thermal actuators were completely defined; however they were still not released from the oxide and silicon surfaces.

5.2.5 Release of the Thermal and Electrostatic Devices

In order to release thermal and electrostatic devices, the "Release Mask: Mask#3" was used to define a 5 micron thick AZ9260 PR. After the development of the PR, the wafer was ready for isotropic etching of silicon, which defines the electrostatic actuator completely. However, there was another required step to release the electrostatic device and thermal actuator fingers. This step was isotropic etching of oxide layers. After the isotropic etching of the oxide layers (thermal oxide, LTO, BPSG, and BOX) below the movable fingers of thermal actuators and movable parts of electrostatic devices, then the complete device was released, and ready for actuation after the stripping of the release mask PR (Figure 5.9).

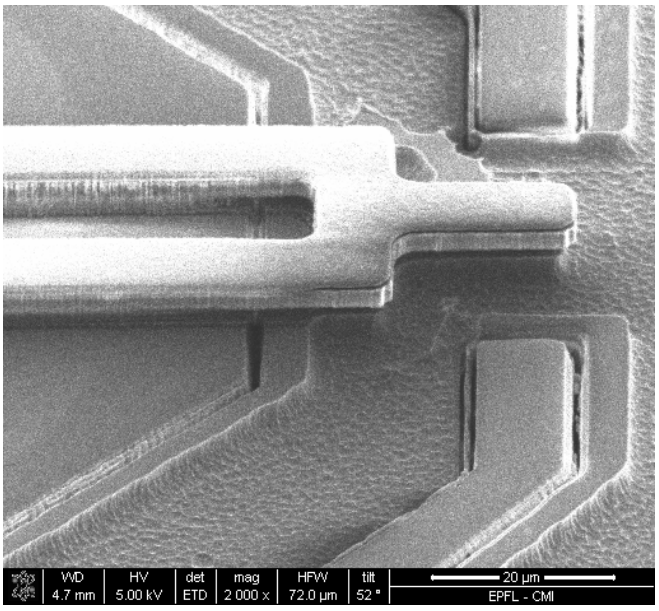

Figure 5. 9: A picture from first generation devices, made on bulk silicon wafer. If this process were performed on an SOI wafer, then the electrostatic and thermal actuators would have been completely released after the isotropic silicon and oxide steps, and removal of the PR from the top surface of both of the devices.

5.2.6 Encountered Problems Related to First Generation Devices

Adhesion between the silicon wafer and AZ9260 after the first photolithographic trial was a problem. We solved it by using an adhesion promoter before spinning the PR on the wafer (Figure 5.10).

Alignment of the 2nd mask with respect to the 1st mask, and alignment of the 3rd mask with respect to the 1st or the 2nd mask was a problem related with the 1st generation devices (Figure 5.11). The basic reason was an error during the design of the alignment marks.

Release of the thermal actuator movable fingers was a problem. We were not able to completely release the movable fingers of the thermal actuators because of calculation and assumption errors during calculation of the etching rates (Figure 5.12, and Figure 5.13).

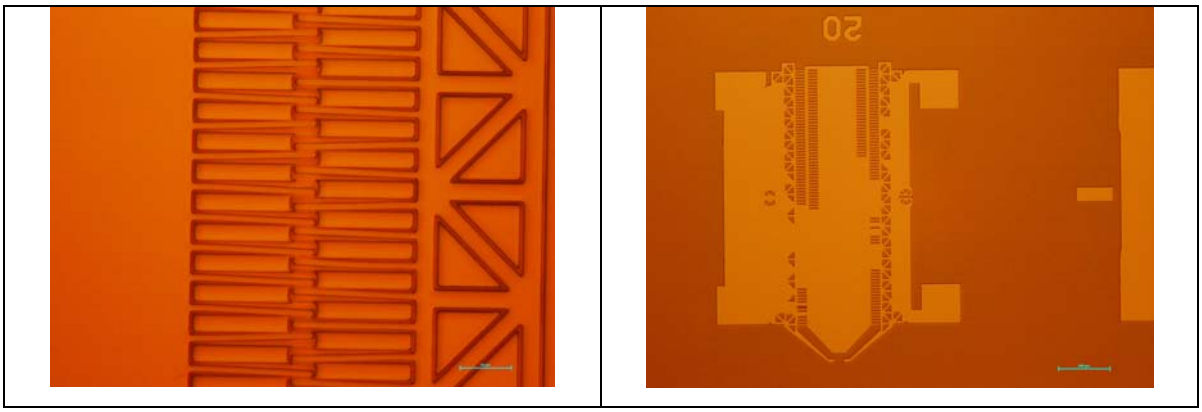

Figure 5. 10: Results of lack of adhesion between the silicon and PR surfaces.

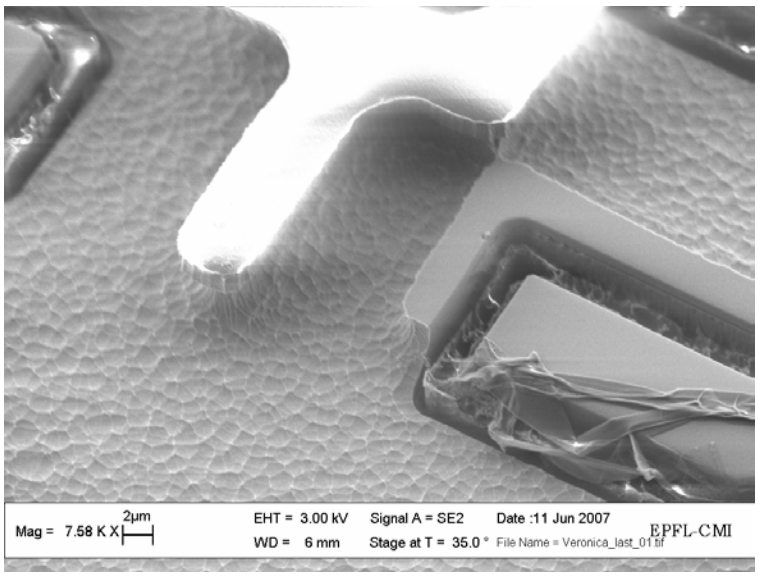

Figure 5. 11: Due to an alignment error, the release mask PR was not completely covering the electrostatic actuator grippers.

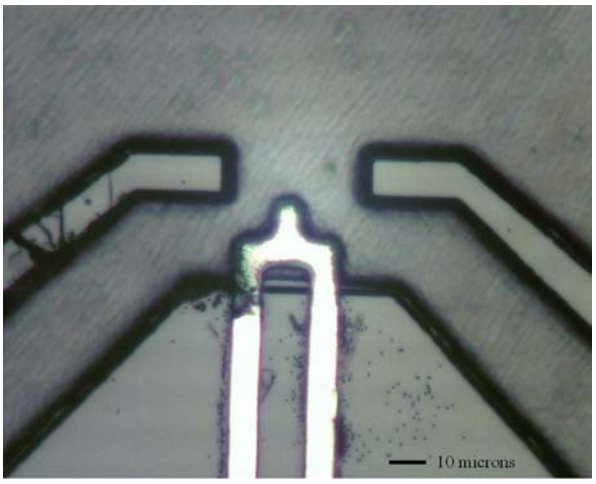

Figure 5. 12: Top view of a thermal actuator that we expected to be released from oxide below its PI layer.

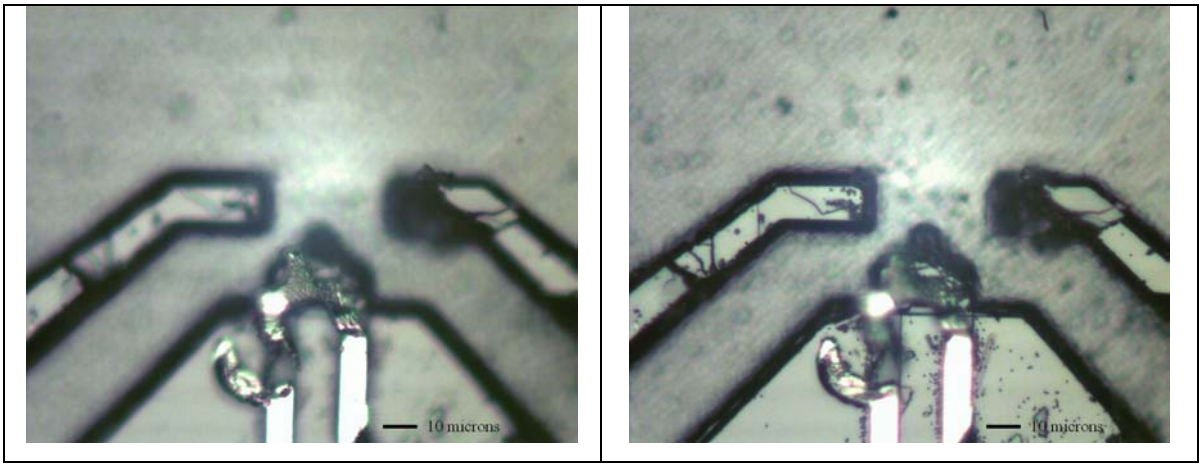

Figure 5. 13: Optical microscope pictures after scratching the tips of the thermal actuators with probe tips. Oxide and silicon layers below thermal actuators, which should have been etched according to the process, were shown by focusing microscope to related surfaces.

Devices with small aluminum line width were not as robust as the devices with wider aluminum line widths. As a solution for this issue, the tips of the thermal actuators were

covered in order to protect the thermal tips from the fluidic forces during the isotropic SILOX etching of oxide layers (Figure 5.14, and Figure 5.15).

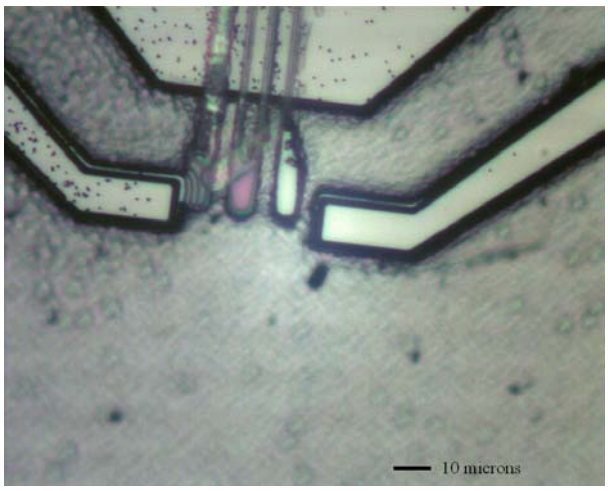

Figure 5. 14: Results from first generation devices, where the thermal actuator movable tips were not protected with the release mask PR from the fluidic forces of the wet isotropic etchant.

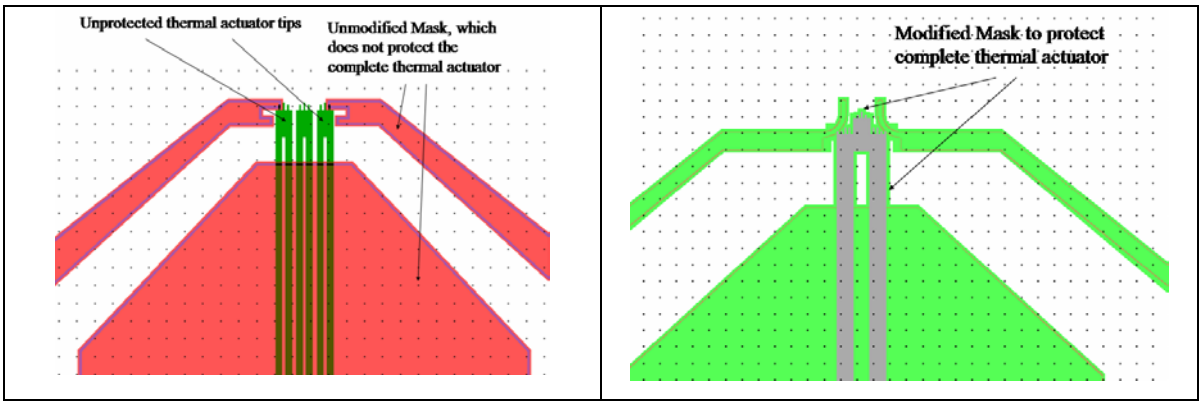

Figure 5. 15: Thermal actuator movable tips are not covered with PR (left). Because of the unreliability due to the fluidic forces, the thermal actuator tips were preserved from the fluidic forces of the isotropic oxide etching by the release mask.

Another problem related with the thermal actuator movable tips was the unexpected etching of aluminum layer of the thermal fingers. SILOX was intentionally used to etch the oxide layers. However, unexpected etching of Aluminum during oxide etch with SILOX directed us to cover the thermal fingers in the second generation of the device fabrication (Figure 5.16).

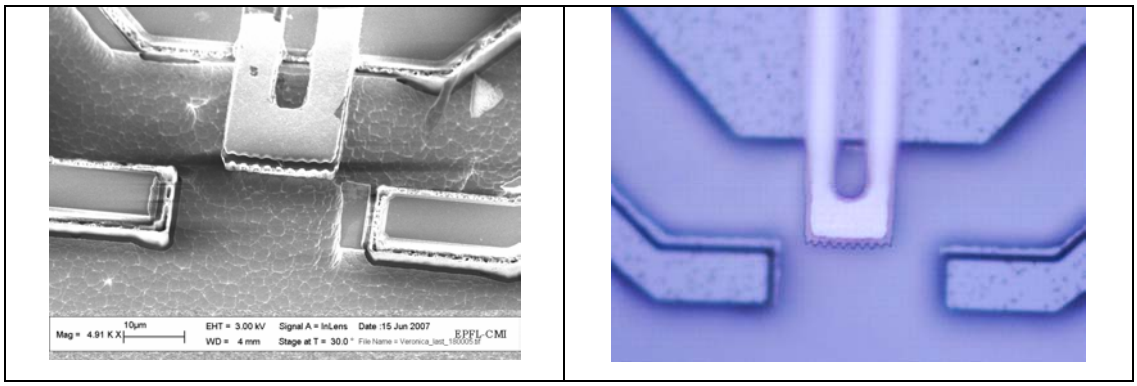

Figure 5. 16: Picture taken in SEM is used to emphasize the region which is etched unexpectedly by SILOX (left), picture taken under optical microscope that shows the unexpected aluminum etching due to SILOX etching (right).

5.3 Technology Development Based Fabrication (2nd Generation)

As it is explained previously, this fabrication is done with SOI wafers, and the aim was to obtain functional thermal and electrostatic actuators with nanometric scale end effectors.

5.3.1 Defining Contours of Electrostatic Devices and Nanowire Integration

The first mask as shown in Figure 5.17 defines device contours and integrated microwires. Here, we call the nanowires as microwires, because wires are still not obtained and are not in sub-micron scale. Next step, after defining the contours on the mask, is directional etching of SOI wafer through the depth of the SOI wafer device thickness in order to obtain the third dimension of the devices (Figure 5.18, and Figure 5.19).

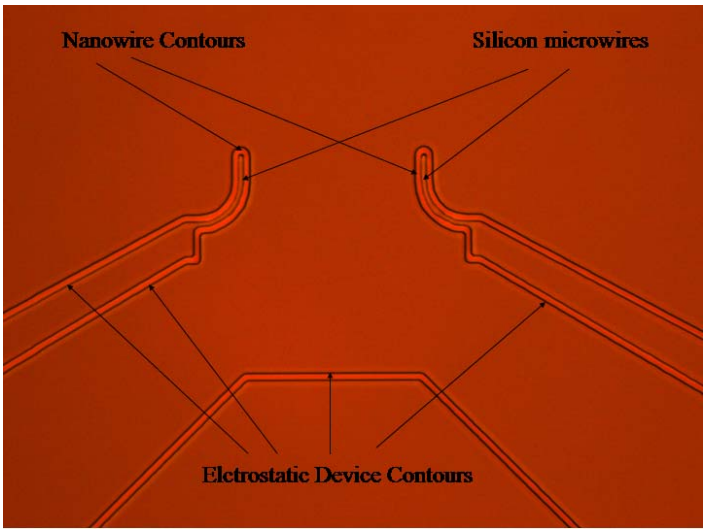

Figure 5. 17: Contours of the devices were defined by using the first mask of the process.

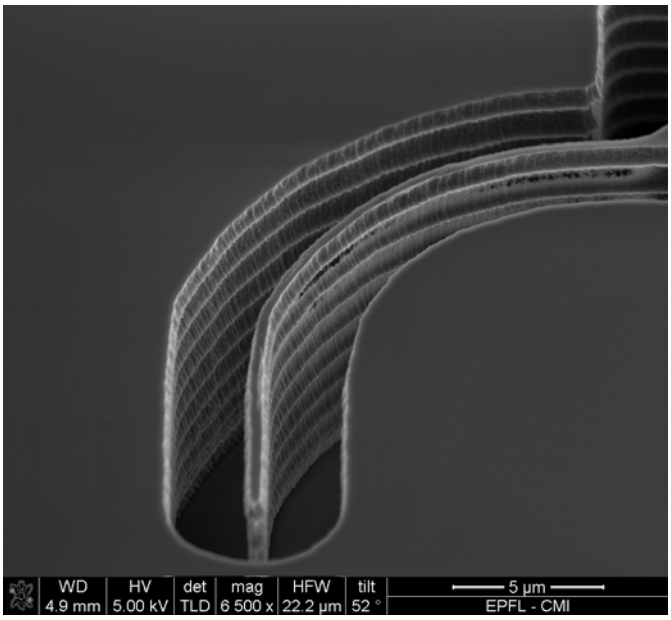

Figure 5. 18: The special DRIE recipe used to obtain the scalloping effect on the stacked nanowires. This process defines the height of the devices through the depth of the SOI wafer.

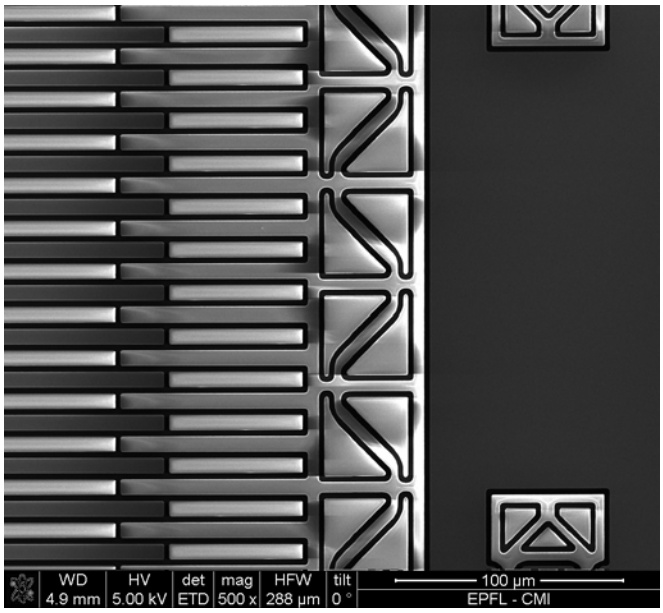

Figure 5. 19: Top view of a device part after the DRIE process. The contours were etched through the depth of the SOI wafer as shown in Figure 5.18.

5.3.2 Defining Thermal Actuators

Before spinning the bottom layer of the thermal actuator, planarization on the SOI wafer surface should be done. There are mainly two reasons to perform this planarization process:

1. The stacked nanowires should be protected from the forces due to the spinning of the photoresists and PI of the next steps, and
2. The wafer surface should be flat to prevent the profile of PI from deterioration due to rough surface during spinning (See Figure 5.20 to understand these 2 entries easily).

Next, the photolithographic steps required for the definition of the thermal actuator mask are performed. This mask is used to etch the upper layer (aluminum) of the thermal actuators. And the remaining PR on aluminum, and the aluminum layer itself was used as a mask for the definition of the bottom layer (PI) of the thermal actuators.

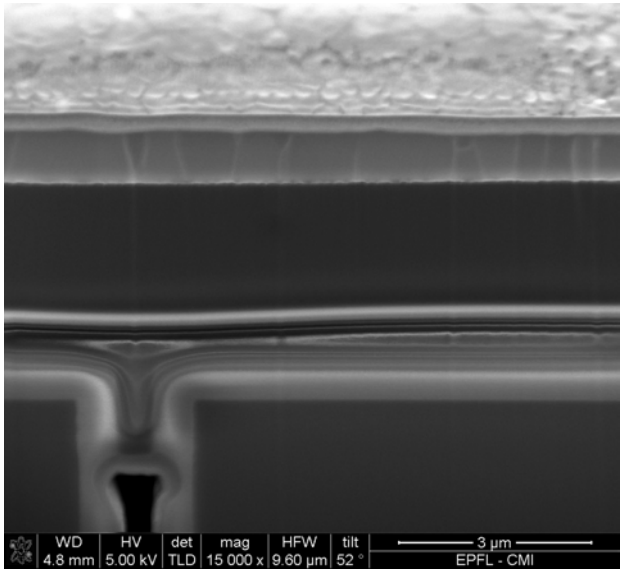

Figure 5. 20: Electrostatic device surface was planarized before the PI and aluminum layers of the thermal actuators were deposited on the surface. The used recipe to planarize the surface was thermal oxidation, LTO deposition, BPSG deposition, and reflow of the oxides at 1050 C°.

After addressing this issue by the successive steps of thermal oxidation, LTO deposition, BPSG deposition, and reflow of the oxides at 1050 C°, bottom layer of thermal actuators is spun and cured. After the PI coating, top surface of the thermal actuators, which is aluminum layer, is evaporated on PI (Figure 5.20).

5.3.3 Release of Devices

After defining the thermal actuators on the oxide surface of the wafer, next steps were to etch the oxide from the surface of the wafers. Directional oxide etching is used to etch the oxide of the wafers. After the directional etching of the oxide on the surface, wafer is ready for the last lithographic step that is designed to release devices from the device silicon layer of an SOI wafer and BOX surface of an SOI wafer. The last lithographic step is performed

with the release mask. After the definition of the mask, dry isotropic silicon etching, and wet isotropic oxide etching were performed in order to release devices from the BOX of SOI wafer. Next, and final, step to clear the devices from the excessive materials of the microfabrication process was the directional etch of the third lithography PR from the upper surface of the devices. Final shape of the electrostatically actuated tips and the thermal actuator fingers are shown in Figure 5.21 and Figure 5.22.

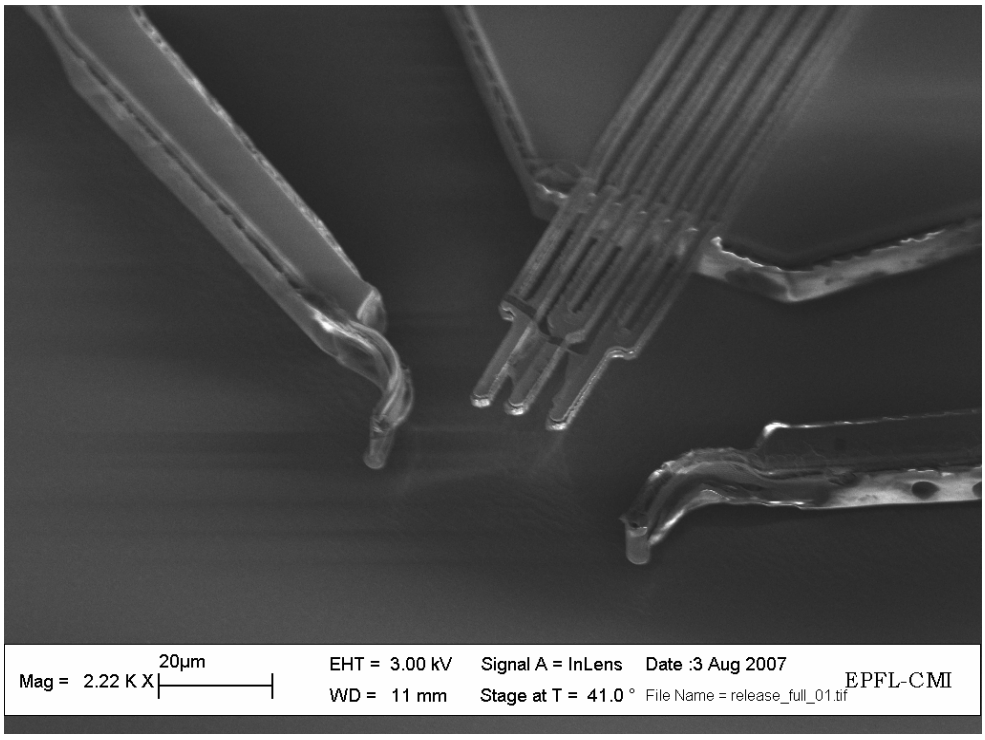

Figure 5. 21: Final shape of the integrated structures after all the process steps were performed.

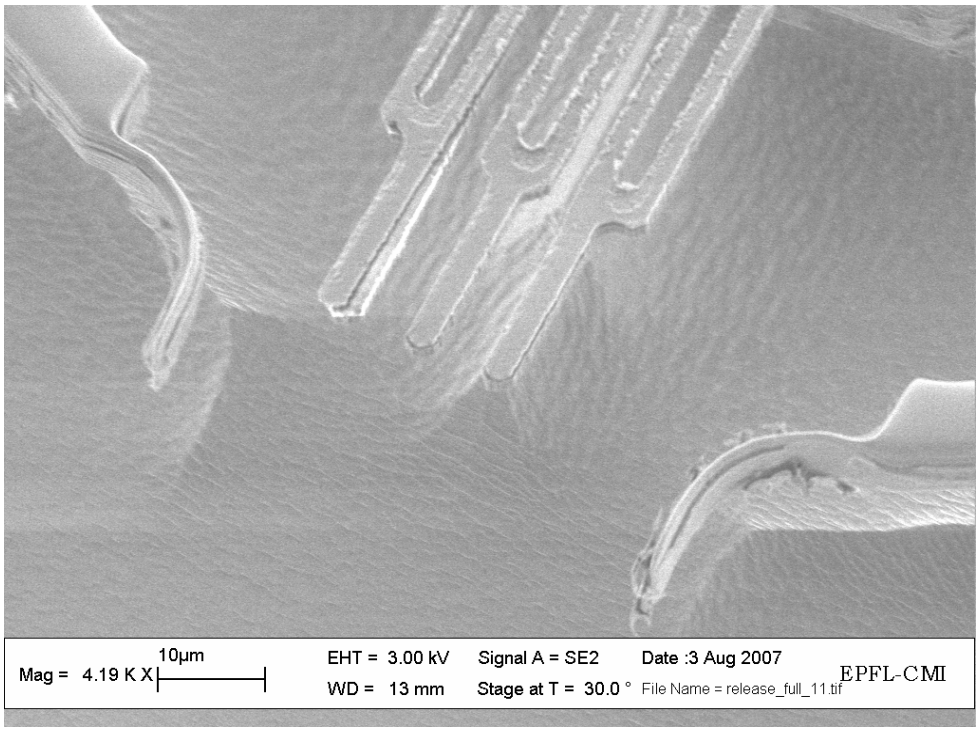

Figure 5. 22: Another view of a device with final shape of the integrated structures after all the process steps were performed.

Chapter 6

CONCLUSIONS

6.1 Conclusions

In this study, we solved micro/nano integration difficulties by proposing three methods and finally demonstrated the simplest, and most time efficient approach as a proof of the proposed idea.

The idea that we used to obtain the nano end-effectors was firstly demonstrated to obtain nanowires by other researchers [4]. However, from another point of view this method was appropriate for nanowire end-effector fabrication and integration to microdevices.

The most serious result of this thesis study was demonstrating a way for the integration of “nano end-effectors” with “microgrippers”. Another serious result of this thesis study was the demonstration of the integration of two different microdevices with different actuation mechanisms to obtain both in-plane and out-of-plane motion types in order to obtain a better gripping action compared to the similar devices with only in-plane motion ability.

Although it is out of scope of this study, this study navigated our research to invent biomedical microdevice applications, which is the next step of the coming group members of Dr. Erdem Alaca. In addition to that, there are many other possible things that can be done related to this project if future researchers spend their time to solve similar problems that explained in this thesis.

If we divide the complete study into two parts, which are design and fabrication based, we can summarize the performed studies as given below.

6.1.1 Design based studies:

The theories of the actuation mechanisms that we use in this study were described. Furthermore, electrostatic actuator and thermal actuator device parameters appropriate for our purposes were chosen, and the reasons to choose these parameters were explained.

Three fabrication sequences for integration of devices with different actuation mechanisms were explained in chapter three. In these sequences, micro/nano integration was proposed, and the reasons to choose the last one as the microfabrication process were given.

The method we followed when we were designing the layout for the microfabrication of the Cr masks, which were used to fabricate the real devices, was presented.

6.1.2 Fabrication based studies:

A lot of hands on experience were gained about different equipments used in microfabrication assembly line, which will be very helpful for the future studies in the field.

The problems encountered during the first generation of the devices were a great lesson about thinking in a deeper manner during the process design phase of the studies.

6.1.3 Proof of integration

This study is a proof of engineered integration of nanostructures to microstructures.

6.2 Discussions

This study was a collaborative study. Mostly, it was a very value adding work, but sometimes due to misunderstandings between the collaborators, it took longer time to complete the study than the expected time. The main misunderstandings were because of the difficulties during the transfer of information between the collaborators.

On the other hand, it was a value adding study because the collaborators were from different disciplines. Thus, there were always different aspects during the discussions and this helped to find better solutions to more complicated problems than only one researcher from only one field of study can think and find a solution.

In this study, the mechanical engineering design algorithm was followed intuitively which helped to approach the problem in a more systematic way. However, if I had the chance to start everything from the beginning, I would not do it intuitively, but I would do it rather more systematic and scheduled [38].

6.3 Some Advice to Future Scientists in the Field of MEMS

This study was like part of my life for the last two years. It was really important to dedicate all my time to this study. Otherwise, it obviously would not be possible to take the research to these aspects.

In a work as wide as this one it is important to plan your time prior to start working. It is important to learn the basics of the field and make the required literature survey before starting to design a device. This will also help defining the slots in the literature and will navigate the research and design specifications.

Never hesitate to ask questions and never consider what people will think if they understand you are not familiar with the work. MEMS is like an ocean. It is not possible to know everything about it. As you go deeper, you always see new things. Or, in other

words, it is like an iceberg. You mostly see the upper part of it, and it takes time to understand the complete volume of the iceberg.

This will be a very cliché sentence, but the truth is that a researcher should not loose his/her motivation when the solution is not found at the beginning. He/She should try to look from different aspects and try to be patient while trying to find a solution, because somehow the solution(s) of the problem is (are) somewhere there, you just need to see it (them)!

BIBLIOGRAPHY

[1] Personal communication with Prof. Bao

[2] V. Pott, D. Grogg, J. Brugger and A. M. Ionescu, Silicon Nanowires Patterning by Sidewall and Nano-Oxidation Processing, Internal publication.

[3] Y. Takahashi, Silicon single-electron devices, J. Phys: Condensed Matter, 14 (2002), R995-R1033.

[4] L. Doherty, h. Liu, V. Milanovic, Application of MEMS Technologies to Nanodevices, Circuits and Systems, 2003. ISCAS apos;03. Proceedings of the 2003 International Symposium on, Volume 3, Issue , 25-28 May 2003 Page(s): III-934 - III-937 vol.3

[5] Chan et al., A thermally actuated polymer micro robotic gripper for manipulation of biological cells, Proceedings of the 2003 IEEE International Conference on Robotics and Automation, Taiwan, 2003, 288-293

[6] Zhou et al., Polymer MEMS Actuators for Underwater Micromanipulation, IEEE/ASME Transactions on Mechatronics, 9(2), (2004) 334-342

[7] Lin et al., Design, Fabrication, and Testing of a C-Shape Actuator, The 8th International Conference on Solid-State Sensors and Actuators, and Eurosensors IX. Stockholm, Sweden, June 25-29, 1995

[8] Sehr et al., Design and Fabrication of a Novel Thermally Actuated Vertical Bimorph Scanner for an Integrated AFM, Part of the Symposium on Design, Test, Integration, and Packaging of MEMS/MOEMS, Proceedings of SPIE Vol. 4019 (2000), 387-397

[9] Ataka et al., Fabrication and Operation of Polyimide Bimorph Actuators for a Ciliary Motion System, J MEMS, 2 (4) (1993) 146-150

[10] Shapiro et al., Bending Actuators with Maximum Curvature and Force and Zero Interfacial Stress, Journal of Intelligent Material Systems and Structures, 0 (2006) 1-6

[11] O. Sardan, Design and Fabrication of Electrostatically Actuated Nanotweezers by Guided Self-assembly, M.Sc. thesis, Koc University, 2006.

[12] S. D. Senturia, Microsystem Design, Kluwer Academic Publishers, (2001).

[13] H. Urey, "ECOE 522 Lecture Notes: Electrostatic Actuators", Koç University, 2004.

[14] John A. Pelesko, David H. Bernstein, Modeling MEMS and NEMS

[15] Michael M. Tilleman, Analysis of electrostatic comb-driven actuators in linear and nonlinear regions, International Journal of Solids and Structures 41 (2004) 4889–4898 [16] W. Huang, G. Lu, Analysis of lateral instability of in-plane comb drive MEMS actuators based on a two-dimensional model, Sensors and Actuators A 113 (2004) 78–85

[17] Y. Sun, D. Piyabongkarn, A. Sezen, B.J. Nelson, and R. Rajamani, A high-aspect-ratio two-axis electrostatic microactuator with extended travel range, Sensors and Actuators A 102 (2002) 49–60

[18] Isabelle P.F. Harouche, C. Shafai, Simulation of shaped comb drive as a stepped actuator for microtweezers application, Sensors and Actuators A 123–124 (2005) 540–546

[19] Ho Nam Kwon, Jong-Hyun Lee, Kazuhiro Takahashi, Hiroshi Toshiyoshi, MicroXY stages with spider-leg actuators for two-dimensional optical scanning, Sensors and Actuators A 130–131 (2006) 468–477

[20] Sayanu Pamidighantam, Robert Puers, Kris Baert, and Harrie A C Tilmans, Pull-in voltage analysis of electrostatically actuated beam structures with fixed–fixed and fixed–free end conditions, J. Micromech. Microeng. 12 (2002) 458–464

[21] Guangya Zhou and Philip Dowd, Tilted folded-beam suspension for extending the stable travel range of comb-drive actuators, J. Micromech. Microeng. 13 (2003) 178–183

[22] J. Li, A.Q. Liu, Q.X. Zhang, Tolerance analysis for comb-drive actuator using DRIE fabrication, Sensors and Actuators A 125 (2006) 494–503

[23] S. Baglio, S. Castorina, L. Fortuna, and N. Savalli, Modeling and Design of novel photo-thermo-mechanical microactuators, Sensors and Actuators A, 101 (2002), 185-193.

[24] Yang et al., An electro-thermal bimorph-based microactuator for precise track-positioning of optical disk drives, Journal of Micromechanics and Microengineering, 15 (2005) 958–965

[25] Boley and Weiner, Theory of Thermal Stresses, 2nd printing, 1962, page: 430

[26] Roark's Formula Book, Chapter 8, Section8.2 "Composite Beams and Bimetallic Strips"

[27] ANSYS 9.0 Tutorial, Chapter 6

[28] Incropera and DeWitt, Fundamentals of Heat and Mass Transfer, 4th Ed., 1996, Natural Convection Chapter

[29] Mills, Heat Transfer, 2nd Ed, 1999, Natural Convection subtopic

[30] A. Atre, Analysis of out-of-plane thermal microactuators, Journal of Micromechanics and Microengineering, 16 (2006) 205–213

[31] Annanthasuresh et al., Comprehensive thermal modeling and characterization of an electrothermal compliant microactuator, Journal of Micromechanics and Microengineering, 11 (2001) 452–462

[32] O. Sardan, A. D. Yalcinkaya and B. E. Alaca, Self-assembly-based batch fabrication of nickel-iron nanowires by electroplating, Nanotechnology 17(9), 2227-2233 (2006)

[33] B. E. Alaca, H. Sehitoglu, and T. Saif, Guided self-assembly of metallic nanowires and channels, Applied Physics Letters 84(23), 4669-4671 (2004)

[34] Williams et al, Etch Rates for Micromachining Processing—Part II, Journal of Microelectromechanical Systems, 12 (6) (2003) 761–778

[35] Islam et al, Ultrahigh-density silicon nanobridges formed between two vertical silicon surfaces, Nanotechnology 15 (2004) L5–L8

[36] HD Microsystems PI2611/10 material bulletin

[37] cmi.epfl.ch

[38] The Practice of Machine Design by Yotaro Hatamura, Oxford University Press

VITA

Mehmet Yılmaz was born in Razgrad, Bulgaria, on 12th of March 1981.

He always dreamed and dreams to be a scientist. As a result, he graduated from Kocaeli Körfez Science High School (Kocaeli Körfez Fen Lisesi, KKFL), in June 2000. Then, he was accepted as a mechanical engineering student to Izmir Institute of Technology (Izmir Yüksek Teknoloji Enstitüsü, IZTECH), and completed his BSc studies with high honors in June 2005. Following his BSc studies, he was accepted as an MSc student to mechanical engineering department of Koç University, under the supervision of Dr. B. Erdem Alaca. During his MSc studies he was specialized in MicroElectroMechanical Systems (MEMS) design and fabrication.

After completing his MSc studies at Koç University, he is going to pursue a PhD degree in mechanical engineering department of Columbia University in the City of New York.